Calhoun: The NPS Institutional Archive

DSpace Repository

Theses and Dissertations | 1. Thesis and Dissertation Collection, all items

2005-06

Modeling and simulation of the physical layer of the single channel ground and airborne radio system (SINCGARS)

Paradise, Richard A.

Monterey, California. Naval Postgraduate School

http://hdl.handle.net/10945/1870

Downloaded from NPS Archive: Calhoun

http://www.nps.edu/library

Calhoun is the Naval Postgraduate School's public access digital repository for research materials and institutional publications created by the NPS community. Calhoun is named for Professor of Mathematics Guy K. Calhoun, NPS's first appointed -- and published -- scholarly author.

Dudley Knox Library / Naval Postgraduate School
411 Dyer Road / 1 University Circle
Monterey, California USA 93943

NAVAL POSTGRADUATE SCHOOL

MONTEREY, CALIFORNIA

THESIS

MODELING AND SIMULATION OF THE PHYSICAL LAYER OF THE SINGLE CHANNEL GROUND AND AIRBORNE RADIO SYSTEM (SINCGARS)

by

Richard Paradise

June 2005

Thesis Advisor:	Frank Kragh
Co-Advisor:	Herschel Loomis

Approved for public release, distribution is unlimited

THIS PAGE INTENTIONALLY LEFT BLANK

REPORT DOCUMENTATION PAGE			Form Approved OMB No. 0704-0188
Public reporting burden for this collection of information is estimated to average 1 hour per response, including the time for reviewing instruction, searching existing data sources, gathering and maintaining the data needed, and completing and reviewing the collection of information. Send comments regarding this burden estimate or any other aspect of this collection of information, including suggestions for reducing this burden, to Washington headquarters Services, Directorate for Information Operations and Reports, 1215 Jefferson Davis Highway, Suite 1204, Arlington, VA 22202-4302, and to the Office of Management and Budget, Paperwork Reduction Project (0704-0188) Washington DC 20503.			
1. AGENCY USE ONLY *(Leave blank)*	**2. REPORT DATE** June 2005	**3. REPORT TYPE AND DATES COVERED** Master's Thesis	
4. TITLE AND SUBTITLE: Modeling and Simulation of the Physical Layer of the Single Channel Ground and Airborne Radio System (SINCGARS)			**5. FUNDING NUMBERS M6890904POH9023**
6. AUTHOR(S) Richard A. Paradise			
7. PERFORMING ORGANIZATION NAME(S) AND ADDRESS(ES) Naval Postgraduate School Monterey, CA 93943-5000			**8. PERFORMING ORGANIZATION REPORT NUMBER**
9. SPONSORING /MONITORING AGENCY NAME(S) AND ADDRESS(ES) Marine Corps Tactical Systems Support Activity Camp Pendleton, CA			**10. SPONSORING/MONITORING AGENCY REPORT NUMBER**
11. SUPPLEMENTARY NOTES The views expressed in this thesis are those of the author and do not reflect the official policy or position of the Department of Defense or the U.S. Government.			
12a. DISTRIBUTION / AVAILABILITY STATEMENT Approved for public release; distribution is unlimited			**12b. DISTRIBUTION CODE**

13. ABSTRACT (maximum 200 words)

In this thesis, the physical layer of the Single Channel Ground and Airborne Radio System (SINCGARS) was analyzed in order to gain insight into the bit-error-rate (BER) performance in various channel conditions. The BER performance of the radio was examined using theoretical, simulation, and experimental techniques. These results are presented in graphical form as the probability of bit error as a function of the energy per bit to noise power spectral density ratio. The results of the simulation show excellent agreement with the theory, while the experimental results deviate from theory at higher signal-to-noise levels. This suggests sub-optimal SINCGARS performance, most notably in the signal power to noise power range where reliable data transmission should take place.

14. SUBJECT TERMS Single Channel Ground and Airborne Radio System, SINCGARS, BFSK, digital communications, faded channels, noncoherent receivers, modeling and simulation			**15. NUMBER OF PAGES** 75
			16. PRICE CODE
17. SECURITY CLASSIFICATION OF REPORT Unclassified	**18. SECURITY CLASSIFICATION OF THIS PAGE** Unclassified	**19. SECURITY CLASSIFICATION OF ABSTRACT** Unclassified	**20. LIMITATION OF ABSTRACT** UL

NSN 7540-01-280-5500 Standard Form 298 (Rev. 2-89)
Prescribed by ANSI Std. 239-18

THIS PAGE INTENTIONALLY LEFT BLANK

Approved for public release; distribution is unlimited

MODELING AND SIMULATION OF THE PHYSICAL LAYER OF THE SINGLE CHANNEL GROUND AND AIRBORNE RADIO SYSTEM (SINCGARS)

Richard A. Paradise
Captain, United States Marine Corps
B.S., Michigan Technological University, 1992

Submitted in partial fulfillment of the
requirements for the degree of

MASTER OF SCIENCE IN ELECTRICAL ENGINEERING

from the

NAVAL POSTGRADUATE SCHOOL
June 2005

Author: Richard A. Paradise

Approved by: Frank Kragh
Thesis Advisor

Herschel H. Loomis
Co-Advisor

John P. Powers
Chairman, Department of Electrical and Computer Engineering

THIS PAGE INTENTIONALLY LEFT BLANK

ABSTRACT

In this thesis, the physical layer of the Single Channel Ground and Airborne Radio System (SINCGARS) was analyzed in order to gain insight into the bit-error-rate (BER) performance in various channel conditions. The BER performance of the radio was examined using theoretical, simulation, and experimental techniques. These results are presented in graphical form as the probability of bit error as a function of the energy-per-bit to noise-power-spectral-density ratio. The results of the simulation show excellent agreement with the theory, while the experimental results deviate from theory at higher signal-to-noise levels. This suggests sub-optimal SINCGARS performance, most notably in the signal-power to noise-power range where reliable data transmission should take place.

THIS PAGE INTENTIONALLY LEFT BLANK

TABLE OF CONTENTS

I. INTRODUCTION....1
A. SINCGARS BACKGROUND....1
1. Model Upgrades....1
B. THESIS FOCUS....2
C. THESIS ORGANIZATION....2

II. SINCGARS OPERATION....3
A. VHF RADIO OVERVIEW....3
B. BASIC OPERATION....4

III. PHYSICAL LAYER ANALYSIS....7
A. RECEIVER MODEL....7
1. FSK Signals....7
2. Noncoherent Quadrature Receiver....8
3. Frequency Hopping – Fast Versus Slow....9
B. PERFORMANCE IN AWGN CHANNEL....10
1. BER for Optimal Noncoherent Detection of BFSK in AWGN....10
2. Noncoherent Quadrature Receiver with Diversity....17
3. BER for Optimal Noncoherent Detection of BFSK in AWGN with Diversity and Hard-Decision Demodulation....20
4. BER for Optimal Noncoherent Detection of BFSK in AWGN with Diversity and Soft-Decision Demodulation....22
C. RICEAN CHANNEL....25
1. Fading Channels....25
a. Parameters....26
b. Types of Fading....27
c. Flat, Slow Fading Criteria....27
2. BER of Noncoherent BFSK over Frequency Non-Selective, Slowly Fading Ricean Channel....29

IV. SIMULATION....33
A. SIMULATION SETUP....33
1. Monte Carlo Method....34
B. SIMULATION RESULTS....35
1. AWGN Channel....35
2. Ricean Channel....36

V. EXPERIMENTAL RESULTS....39
A. LABORATORY SETUP....39
1. Main Components....40
B. LABORATORY PROCEDURE....43
1. Experiment A....43
2. Experiment B....45

C. LABORATORY RESULTS AND DISCUSSION 45
1. Experiment A and B Results 45
2. Discussion 48
a. Performance and Range 50
VI. CONCLUSION AND FUTURE WORKS 53
A. CONCLUSION 53
B. FUTURE WORK 54
LIST OF REFERENCES 55
INITIAL DISTRIBUTION LIST 57

LIST OF FIGURES

Figure 1. VHF Radio Block Diagram 3
Figure 2. Noncoherent BFSK Receiver Block Diagram 9
Figure 3. BER for Noncoherent BFSK in AWGN 17
Figure 4. Noncoherent BFSK Hard-Decision Receiver 19
Figure 5. Noncoherent BFSK Soft-Decision Receiver 20
Figure 6. Noncoherent BFSK with Diversity and Hard-Decision Demodulation 22
Figure 7. BER for Noncoherent BFSK with Diversity – Hard vs Soft Decision Demodulation 25
Figure 8. BER for Noncoherent BFSK in Frequency Non-Selective, Slow Fading Channel 32
Figure 9. Simulink Model BFSK System in AWGN 33
Figure 10. BER for BFSK in AWGN Channel via Simulation and Analysis 36
Figure 11. BER for Noncoherent BFSK in Ricean Channel via Simulation and Analysis 38
Figure 12. Experiment Overview 39
Figure 13. Laboratory Setup – Block Diagram 40
Figure 14. Laboratory Setup - Photo 41
Figure 15. PXI-1042 42
Figure 16. SCB-68 and Break-Out Box 42
Figure 17. Attenuators 42
Figure 18. SINCGARS 43
Figure 19. Noise Generator 43
Figure 20. Experiment A Results 46
Figure 21. Experiment A Results: Deviation from Analytical 47
Figure 22. Experiment A and B Results Comparison 48
Figure 23. Comparison of Experimental Results – Experiment B Results Adjusted 49

THIS PAGE INTENTIONALLY LEFT BLANK

LIST OF TABLES

Table 1. SINCGARS Specifications 5
Table 2. Simulink Model Block Description 34
Table 3. Experiment A Results 45

THIS PAGE INTENTIONALLY LEFT BLANK

ACKNOWLEDGMENTS

First and foremost, I would like to thank my wife for her love and support during our time here at the Naval Postgraduate School. Her devotion to her family is truly inspirational. I would also like to express my sincere gratitude to Prof. Frank Kragh for his role as my thesis advisor and for the technical guidance and knowledge he provided throughout the thesis process.

Finally, I would like to thank the Marine Corps Tactical System Support Activity (MCTSSA) for the thesis idea and funding.

THIS PAGE INTENTIONALLY LEFT BLANK

EXECUTIVE SUMMARY

The ability to reliably and rapidly communicate data over a Very High Frequency (VHF) radio channel at the tactical level of today's battlefield is becoming increasingly important. Field radios are no longer used for just analog voice communications, but are now moving data and being used as integral components of data networks. In the U.S. military, the Single Channel Ground and Airborne Radio System (SINCGARS) plays a significant role in tactical VHF terrestrial communication and, as such, its ability to manipulate data is critical to the effective flow of information on the battlefield. Concerns regarding poor performance in tactical VHF data communication as a whole have lead to a closer examination of the SINCGARS and possible flaws in the data transmission path through the radio [1].

This thesis examines the physical layer of the SINCGARS in order to gain insight into its performance. This was done by first developing an optimal model of the radio and then deriving the theoretical bit-error-rate equations for the additive-white–Gaussian-noise (AWGN) and fading-channel cases. Next, a computer simulation of the radio model was performed using MATLAB and Simulink. Again, as with the theoretical derivations, the simulation was run for both channel assumptions. Finally, bit-error-rate data was collected in the laboratory by transmitting a stream of data bits from one SINCGARS to another over a wire channel. The laboratory setup included a voltage-controlled AWGN generator which allowed for varying levels of noise power and an application that compared the received bit stream to the transmitted bit steam and counted the errors.

Although the simulation results showed excellent agreement with theory, the experimental results suggest that the radio is performing at a sub-optimal level. Additionally, the results show that the deviation from optimal performance increases at higher signal-to-noise ratios and in the bit-error-rate range where reliable data communications should take place.

THIS PAGE INTENTIONALLY LEFT BLANK

I. INTRODUCTION

A. SINCGARS BACKGROUND

Since its introduction in the mid 1980s, the Single Channel Ground and Airborne Radio System (SINCGARS) family of radios has served its role as a main component in the U.S. military's tactical communications. They were designed to replace the AN/PRC-25/77 and AN/VRC-12 family of radios and provide both voice and data transmission capability. SINCGARS operates in the Very High Frequency (VHF) band and utilizes frequency modulation (FM). Information can be transmitted and received in either a single-channel or frequency-hopping mode depending on the electronic countermeasures environment. The radio's modular design allows for commonality between lightweight manpack, vehicular, and airborne versions, with the heart of the system being a common receiver/transmitter (RT). While seeking to improve upon the basic operational concepts of the original SINCGARS, many upgraded models have been introduced since its inception [2].

1. Model Upgrades

Over the years, a number of significant enhancements have been made to the SINCGARS family of radios. The original model provided for non-secure frequency-hopping voice communication and required an external KY-57 transmission security device for secure operation. This external KY-57 device provided voice and data encryption prior to modulation by the radio and is considered communication security (COMSEC) equipment because it denies access to the information by unauthorized users. The first major upgrade integrated the COMSEC (encryption) equipment into the body of the radio and also addressed the growing need to communicate not only voice, but also data around the battle space. This integrated COMSEC (ICOM) version of the SINCGARS was followed by system improvement programs (SIP) that enhanced the radios' performance and networking capability. Changes resulting from the improvement programs allowed for forward error correction coding, automatic network radio interfacing, Global Positioning System functionality, as well as packet data capabilities. Ad-

vanced SIP radios continue the trend of improving data communication performance, as well as increasing battery life and reducing the size (and weight) of the system.[3]

B. THESIS FOCUS

As the history of the SINCGARS upgrades shows, the focus is on improving the data communications ability of the radio. This underscores a shift on the battlefield from predominately voice communication to data communication. With this shift to data communications comes the need for better bit-error-rate (BER) performance, as the requirement in BER is more stringent for data as compared to voice. Concerns regarding poor performance in tactical VHF data communication as a whole have lead to a closer examination of the SINCGARS and possible inefficiencies in the data transmission path through the radio [1]. It is the need to improve data communications performance that drives us to examine the SINCGARS herein.

C. THESIS ORGANIZATION

Chapter II of the thesis describes the basic operation of the SINCGARS and lists some general performance characteristics.

Chapter III covers the physical layer analysis and includes the derivation of bit error rates for differing channels and under varying diversity schemes.

Chapter IV covers the simulation of the physical layer model and compares with Chapter III results.

Chapter V describes the laboratory setup and lists the results. It also compares the laboratory data with the previous chapters' theoretical and simulation results.

Chapter VI summarizes the findings in the thesis and provides recommendations for future work.

II. SINCGARS OPERATION

A. VHF RADIO OVERVIEW

The Very High Frequency (VHF) spectrum ranges from 30 to 300 MHz. In this frequency range, the electromagnetic energy generated will have wavelengths between 1 and 10 meters as shown below.

$$\lambda = \frac{c}{f} = \frac{3\times10^{8}\ \text{m/s}}{300\times10^{6}\ \text{s}^{-1}} = 1\ \text{meter},$$
$$\lambda = \frac{c}{f} = \frac{3\times10^{8}\ \text{m/s}}{30\times10^{6}\ \text{s}^{-1}} = 10\ \text{meters}. \tag{2.1}$$

Shorter wavelengths translate to smaller electronic components and shorter antennas, two preferred characteristics of radios used in a tactical field environment.

A block diagram of the main components of a typical VHF radio is shown in Figure 1.

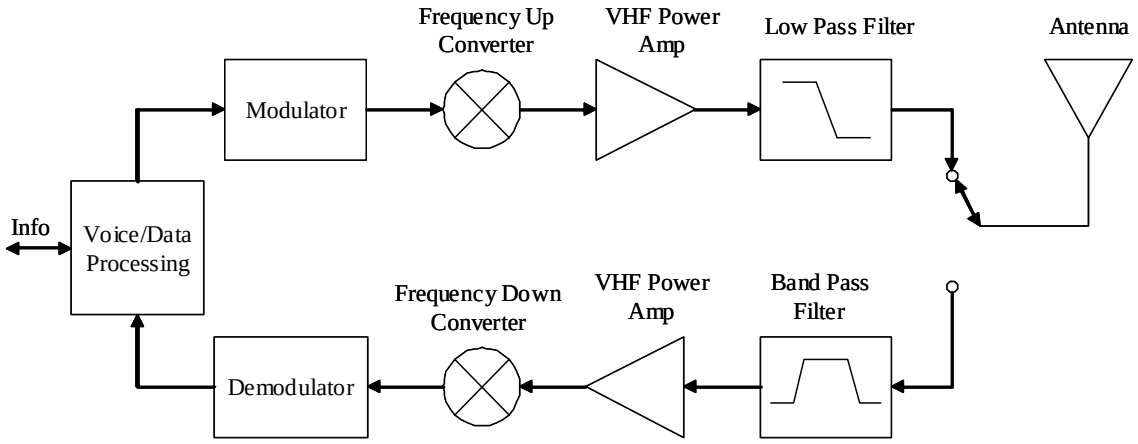

Figure 1. VHF Radio Block Diagram (After [4].)

Transmit and receive operations within the radio are reciprocal. In some radios, the voice and data processing as well as the modulation and demodulation functions are accomplished through the use of a digital signal processor (DSP). Basically a small computer,

the DSP performs filtering, analog-to-digital (A/D) conversion, data encryption, data encoding for forward error correction, and finally modulation. At the output of the modulator, the signal is at an intermediate frequency (IF) and is a low frequency representation of the original information. This signal is then up-converted to the appropriate carrier frequency, amplified, filtered, and transmitted via the antenna. Reception of a VHF signal is processed in the reverse order.[4]

B. BASIC OPERATION

The SINCGARS can operate in single-channel or frequency-hopping modes and is capable of transmitting both voice and data. Operation is in the frequency range from 30 to 87.975 MHz, with an internal IF frequency of 12.5 MHz. Within this operating frequency range, the radio has 2,320 25-kHz channels available for use in both modes. For data communications, the radios utilize Binary Frequency Shift Keying (BFSK) modulation. For voice communications, the radios use analog FM with a frequency deviation of 6.5 kHz.[5] During frequency hopping, symbols are transmitted on a channel randomly selected by a pseudo-noise (PN) sequence generator with the channel frequency hopping at a pre-determined rate of "about 100 times per second" [3]. The older SINCGARS models employ repetition coding while the SIP radios are backward compatible and capable of forward error correction (FEC) utilizing Reed-Solomon codes. In order to accommodate the improved features and backward compatibility, two modes of operation are available for the user to select. The SINCGARS Data Mode (SDM) provides backward compatibility with the older model radios while the Enhanced Data Mode (EDM) can be selected to take advantage of the improved FEC [6]. Data transmission rates range from 600 bps to 16 kbps [2]. Table 1 summarizes the performance characteristics.

This chapter provided an overview of the operation of a VHF radio and presented the basic operation of the SINCGARS. The next chapter will analytically examine the SINCGARS performance.

Frequency Range	30.0-87.975 MHz
Modulation Type	FM Voice BFSK Data
Intermediate Frequency	12.5 MHz
FM Voice Frequency Deviation	6.5 kHz
Modes	Single Channel Frequency Hopping
Number of Channels	2320
Channel Spacing	25 kHz
Data Transmission Rate	600 bits/sec – 16kbits/sec
Coding	Repetition/Reed Soloman
Power Output	0.5 mW, 160 mW,5 or 50 W (with power amp)

Table 1. SINCGARS Specifications [2,3,5]

THIS PAGE INTENTIONALLY LEFT BLANK

III. PHYSICAL LAYER ANALYSIS

This chapter analytically examines the performance of the SINCGARS modeled as a slow-frequency-hopping, BFSK system utilizing noncoherent detection. The probability of bit error is derived for various channel assumptions and levels of diversity. Also, a comparison of two techniques for determining the decision statistic when diversity is present is made.

A. RECEIVER MODEL

1. FSK Signals

In a digital communication system, information is represented as a stream of binary digits or bits. These bits are grouped together to form a finite set of M symbols to which the system can map the information. For a binary symbol set, $M = 2$ and each symbol represents one bit and thus a total of two symbols are generated. The receiver and transmitter must employ a modulation scheme that enables the receiver to distinguish between the two symbols.[7]

M-ary Frequency Shift Keying (MFSK) is a digital modulation technique where each of the symbols is represented by a sinusoidal pulse at one of M distinct frequencies. The general expression for an MFSK signal is [7]

$$s_i(t) = \begin{cases} \sqrt{\frac{2E}{T_b}} \cos(\omega_i t + \theta) & 0 \le t \le T_b, \;\; i = 1, \ldots, M \\ 0 & t \notin [0, T_b] \end{cases} \tag{3.1}$$

where

$i = 1, \ldots, M$ identifies the symbols,

ω_i is the frequency of the i^{th} symbol,

T_b is the symbol duration,

E is the energy in the signal during a single symbol duration T_b and

θ is the signal phase.

If the receiver determines the phase of the signal, the reception process is referred to as coherent detection. Otherwise, the receiver utilizes noncoherent detection [7].

Real signals, s_1 and s_2, in a symbol set are called orthogonal over one symbol duration if they satisfy the Equation [7]

$$\int_0^{T_b} s_1(t)\, s_2(t)\, dt = 0. \tag{3.2}$$

For noncoherent FSK, it can be shown that the criteria in Equation 3.2 will be satisfied when the signals in the symbol set are separated in frequency by a minimum of $\Delta f = 1/T_b$ [7]. Therefore, for BFSK with orthogonal signaling and noncoherent detection, the symbols can be represented by the equation [8]

$$s_i(t) = \begin{cases} \sqrt{2}A\cos\left[\left(\omega_c \pm \dfrac{\Delta\omega}{2}\right)t + \theta\right] & 0 \le t \le T_b,\ i = 1,2 \\ 0 & t \notin [0, T_b] \end{cases} \tag{3.3}$$

where

ω_c is the carrier frequency,

$\Delta\omega$ is the symbol frequency separation, and

A is the signal root mean squared amplitude and $\sqrt{2E/T_b} = \sqrt{2A^2} = \sqrt{2}A$.

2. Noncoherent Quadrature Receiver

A noncoherent BFSK detector can be implemented with correlators and squaring operators as shown in Figure 2.

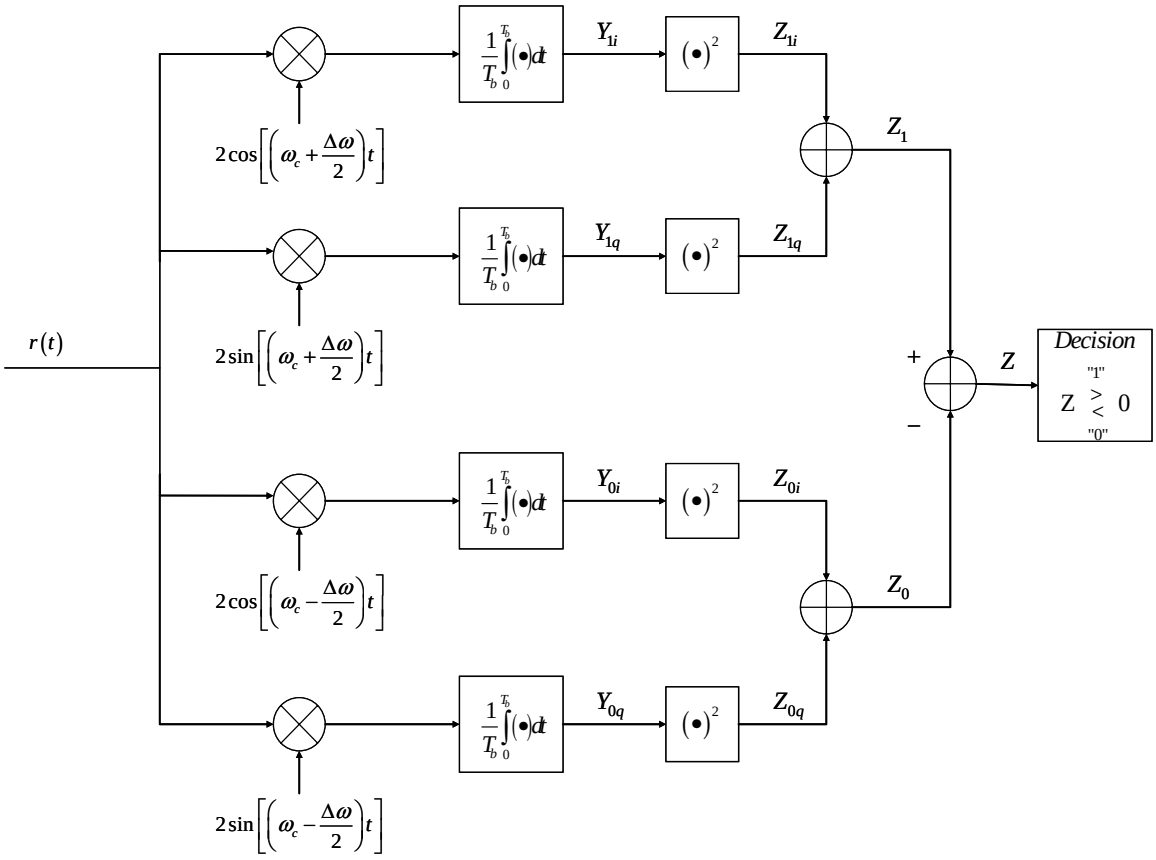

Figure 2. Noncoherent BFSK Receiver Block Diagram (After [9].)

The decision statistic at the output compares the amount of energy detected from each dual branch of the receiver. Each dual detector branch is matched to one of the two symbols. Because there is no knowledge of the signal's phase, two paths per symbol are needed. These are called the inphase (I) and quadrature (Q) detectors. The received signal is first correlated with the I and Q oscillators, with the results squared and then added to remove the phase information. A decision is made by choosing the symbol detector branch that produced the larger value. This type of receiver is also known as a quadrature detector.[9]

3. Frequency Hopping – Fast Versus Slow

Frequency hopping is a spread spectrum technique where the carrier frequency is no longer fixed, but is instead selected (hopped) pseudo-randomly. If the time interval between hops is less than the symbol duration, the system is considered fast-frequency hopping. This means that a single symbol will be transmitted using more than one carrier

frequency. On the other hand, if the time between hops is greater than the symbol duration, the system is considered slow-frequency hopping. In other words, multiple consecutive symbols will be transmitted utilizing the same carrier frequency [7]. For BFSK with orthogonal signaling and noncoherent detection, incorporating slow-frequency hopping will not change the performance in an AWGN channel, whereas fast-frequency hopping will degrade the BER performance [11].

For the SINCGARS, the frequency hopping rate is "about 100 times per second" [3]. In other words, the carrier frequency changes approximately every 10 ms. At 16 kbps, the symbol period for binary data communications is $1/16\text{x}10^3 = 62.5\ \mu\text{s}$. Therefore, at each hopped carrier frequency approximately 160 bits are transmitted. This satisfies the criteria for slow-frequency hopping.

B. PERFORMANCE IN AWGN CHANNEL

1. BER for Optimal Noncoherent Detection of BFSK in AWGN

If we assume that the received signal is corrupted by additive white Gaussian noise (AWGN), the input to the receiver can be represented by one of the following two signals [8]

$$r(t) = \begin{cases} s_1(t) + n(t) = \sqrt{2}A\cos\left[\left(\omega_c + \dfrac{\Delta\omega}{2}\right)t + \theta\right] p_{T_b}(t) + n(t) \\ s_0(t) + n(t) = \sqrt{2}A\cos\left[\left(\omega_c - \dfrac{\Delta\omega}{2}\right)t + \theta\right] p_{T_b}(t) + n(t) \end{cases} \quad 0 \le t \le T_b \qquad (3.4)$$

where

T_b is the bit interval or symbol duration,

$n(t)$ is AWGN with power spectral density $N_0/2$,

$p_{T_b}(t) = \begin{cases} 1 & \text{if } t \in [0, T_b] \\ 0 & \text{otherwise} \end{cases}$, and

θ is the unknown phase at the receiver.

Following the procedures outlined in Reference [8] and referring to Figure 2, the initial goal is to determine the probability density function (PDF) at the decision block input. Because the multipliers and integrators are linear operators, the signal and noise components can be analyzed separately up to the input of the square-law device. Assuming $s_1(t)$ is sent, the integrator output in the I channel of the top dual branch due to the signal only is

$$Y_{1i}(T_b) = \frac{2\sqrt{2}A}{T_b}\int_0^{T_b} \cos\left[\left(\omega_c + \frac{\Delta\omega}{2}\right)t + \theta\right]\cos\left[\left(\omega_c + \frac{\Delta\omega}{2}\right)t\right]\, dt. \tag{3.5}$$

Using the trigonometric identity

$$\cos A \cos B = \frac{1}{2}\cos(A+B) + \frac{1}{2}\cos(A-B) \tag{3.6}$$

Equation 3.5 becomes

$$Y_{1i}(T_b) = \frac{\sqrt{2}A}{T_b}\int_0^{T_b} \cos\left[\left(2\omega_c + \Delta\omega\right)t + \theta\right] + \cos\left(\theta\right)\, dt. \tag{3.7}$$

If we assume $\omega_c \gg 1/T_b$, or equivalently $f_c \gg R_b$ where R_b is the bit rate, then evaluating Equation 3.7 results in

$$Y_{1i}\left(T_b\right) = \sqrt{2}A\cos\left(\theta\right). \tag{3.8}$$

Similarly, the integrator output of the quadrature channel in the top dual branch due only to the signal part of $r(t)$ is

$$Y_{1q}\left(T_b\right) = -\sqrt{2}A\sin\left(\theta\right). \tag{3.9}$$

Now consider the response of the detector branches that are not matched to the signal $s_1(t)$. The I channel integrator output is

$$Y_{0i}\left(T_b\right) = \frac{2\sqrt{2}A}{T_b}\int_0^{T_b} \cos\left[\left(\omega_c + \frac{\Delta\omega}{2}\right)t + \theta\right]\cos\left[\left(\omega_c - \frac{\Delta\omega}{2}\right)t\right]\, dt. \tag{3.10}$$

Again using the trigonometric identity in Equation 3.6, Equation 3.10 becomes

$$Y_{0i}(T_b) = \frac{\sqrt{2}A}{T_b}\int_0^{T_b} \cos(2\omega_c t + \theta) + \cos(\Delta\omega t + \theta)\, dt. \tag{3.11}$$

Carrying out the integration and again assuming $\omega_c \gg R_b$ results in

$$Y_{0i}(T_b) = \frac{\sqrt{2}A}{T_b}\left[\left(\frac{1}{\Delta\omega}\sin(\Delta\omega T_b + \theta)\right) - \left(\frac{1}{\Delta\omega}\sin(\theta)\right)\right]. \tag{3.12}$$

This leads to

$$Y_{0i}(T_b) = 0 \tag{3.13}$$

when $\Delta\omega T_b = 2\pi n$ or $\Delta f = n/T_b = nR_b$. This is the required frequency separation for optimal noncoherent detection of FSK using orthogonal signaling. Similarly, the integrator output of the bottom dual branch Q channel, due only to the signal portion of $r(t)$, is

$$Y_{0q}(t) = 0. \tag{3.14}$$

Now that the signal portion of $r(t)$ has been examined through the output of the integrators, we now examine the noise, i.e. $r(t) = n(t)$. Starting with the output of the multiplier in the top branch, we write the mixer output as

$$m(t) = 2n(t)\cos\left[\left(\omega_c + \frac{\Delta\omega}{2}\right)t\right] \tag{3.15}$$

where $n(t)$ is AWGN. From the definition of the autocorrelation function,

$$R_m(t, t+\tau) = \mathrm{E}\left[\left(2n(t)\cos\left[\left(\omega_c + \frac{\Delta\omega}{2}\right)t\right]\right)\left(2n(t+\tau)\cos\left[\left(\omega_c + \frac{\Delta\omega}{2}\right)(t+\tau)\right]\right)\right] \tag{3.16}$$

where $\mathrm{E}[\cdot]$ denotes the expected value. Let $\omega_0 = \omega_c + \Delta\omega/2$ and using the trig identity in Equation 3.6 to rewrite Equation 3.16 as

$$R_m(t, t+\tau) = \mathrm{E}\left[\left[2n(t)n(t+\tau)\right]\left[\cos(2\omega_0 t + \omega_0\tau) + \cos(\omega_0\tau)\right]\right]. \tag{3.17}$$

This can be reduced to

$$R_m(t,t+\tau) = 2R_n(\tau)\left[\cos(2\omega_0 t + \omega_0\tau) + \cos(\omega_0\tau)\right]. \tag{3.18}$$

Next, using the relationship between the power spectral density (PSD) and the Fourier transform of the autocorrelation, Equation 3.18 can be written

$$S_m(f) = \mathrm{F}\left\langle 2R_n(\tau)\left[\cos(2\omega_0 t + \omega_0\tau) + \cos(\omega_0\tau)\right]\right\rangle \tag{3.19}$$

where $\langle\cdot\rangle$ denotes time average with respect to t and $\mathrm{F}[\cdot]$ denotes the Fourier transform. Therefore

$$S_m(f) = \mathrm{F}\left[2R_n(\tau)\cos(\omega_0\tau)\right]. \tag{3.20}$$

Applying the Fourier transform pair

$$\cos(2\pi f_0\tau) \overset{\mathrm{F}}{\longleftrightarrow} \frac{1}{2}\delta(f - f_0) + \frac{1}{2}\delta(f + f_0) \tag{3.21}$$

yields the relationship

$$2R_n(\tau)\cos(\omega_0\tau) \overset{\mathrm{F}}{\longleftrightarrow} 2S_n(f) * \left[\frac{1}{2}\delta(f - f_0) + \frac{1}{2}\delta(f + f_0)\right] \tag{3.22}$$

where $*$ denotes convolution. Using Equations 3.20 and 3.22 and substituting the PSD of the AWGN, the PSD at the output of the multiplier is

$$S_m(f) = S_n(f - f_0) + S_n(f + f_0) = \frac{N_0}{2} + \frac{N_0}{2} = N_0. \tag{3.23}$$

In other words, white noise into the multiplier results in white noise out.

Applying the results of Equation 3.23 to the integrator, and utilizing the relationship

$$S_y(f) = \left|H(f)\right|^2 S_x(f) \tag{3.24}$$

where

$S_x(f) = N_0$, $S_x(f)$ is the PSD at the integrator input,

$S_y(f)$ is the PSD at the integrator output,

$H(f)$ is the Fourier transform of the impulse response of the integrator, and

$|H(f)|^2$ is the power transfer function

results in

$$S_y(f) = |H(f)|^2 N_0. \tag{3.25}$$

Using Parseval's Theorem, $\int_{-\infty}^{\infty} |H(f)|^2 df = \int_{-\infty}^{\infty} |h(t)|^2 dt$, the integrator output can be related to the noise power as

$$\sigma_y^2 = \int_{-\infty}^{\infty} S_y(f) = N_0 \int_{-\infty}^{\infty} |H(f)|^2 df = N_0 \int_{-\infty}^{\infty} |h(t)|^2 dt \tag{3.26}$$

It can be shown [8] that the impulse response of the integrator in Figure 2 is

$$h(t) = \frac{1}{T_b} \int_{t-T_b}^{t} \delta(\beta) d\beta = \begin{cases} \frac{1}{T_b} & \text{for } 0 < t < T_b \\ 0 & \text{otherwise.} \end{cases} \tag{3.27}$$

Therefore Equation 3.26 reduces to

$$\sigma_y^2 = N_0 \int_0^{T_b} \left(\frac{1}{T_b} \right)^2 dt = \frac{N_0}{T_b}. \tag{3.28}$$

The above noise analysis shows that zero-mean-Gaussian noise at the input results in zero-mean-Gaussian noise with variance N_0/T_b at the integrator outputs.

Combining the results of Equations 3.8, 3.9, and 3.28, we see that the PDFs of the integrator outputs in the receiver branches matched to the input signal are Gaussian random variables with means given in Equations 3.8 and 3.9 and with a variance $\sigma^2 = N_0/T_b$. Similarly, using the results of Equations 3.13, 3.14, and 3.28, the PDFs of

the integrator outputs in the receiver branches not matched to the received signal are zero-mean Gaussian random variables with variance $\sigma^2 = N_0/T_b$. The PDFs are

$$p_{y_{1i}}(y) = \frac{1}{\sqrt{2\pi}\sigma} e^{-\frac{\left(y-\sqrt{2}A\cos\theta\right)^2}{2\sigma^2}} \tag{3.29}$$

$$p_{y_{1q}}(y) = \frac{1}{\sqrt{2\pi}\sigma} e^{-\frac{\left(y+\sqrt{2}A\sin\theta\right)^2}{2\sigma^2}} \tag{3.30}$$

$$p_{y_{0i}}(y) = \frac{1}{\sqrt{2\pi}\sigma} e^{-\frac{y^2}{2\sigma^2}} \tag{3.31}$$

and

$$p_{y_{0q}}(y) = \frac{1}{\sqrt{2\pi}\sigma} e^{-\frac{y^2}{2\sigma^2}}. \tag{3.32}$$

As described in Reference [9], the PDFs of the outputs of the square-law devices are central or noncentral chi-squared random variables of degree 1. The random variable Z_1 represents the output of the receiver branch matched to the input signal and is non-central chi-squared of degree 2. The random variable Z_0 is the output from the branch not matched to the input signal and is central chi-squared of degree 2 (also known as an exponential random variable). The PDFs for Z_0 and Z_1 are

$$p_{Z_1}(z_1) = \frac{1}{2\sigma^2} e^{-\frac{\left(z_1+2A^2\right)}{2\sigma^2}} I_0\left(\frac{\sqrt{2A^2 z_1}}{\sigma^2}\right) u(z_1) \tag{3.33}$$

and

$$p_{Z_0}(z_0) = \frac{1}{2\sigma^2} e^{-\frac{z_0}{2\sigma^2}} u(z_0) \tag{3.34}$$

where

$\sigma^2 = N_0/T_b$,

$I_0(z)$ is the modified Bessel function of the first kind and order zero, and

$u(z)$ is the unit step function.

Again assuming $s_1(t)$ was sent, a detection error will occur when $Z < 0$ or $Z_1 < Z_0$.

$$\Pr[\text{error} \mid s_1 \text{ sent}] = P_{b|1} = \Pr[Z < 0 \mid s_1] = \Pr[Z_1 - Z_0 < 0 \mid s_1] = \Pr\left[Z_1 < Z_0 \mid s_1\right]. \quad (3.35)$$

Following the derivation in Reference [10], the conditional PDF can be expressed as

$$P_{b|1} = \iint\limits_{z_1 < z_0} p_{Z_0 Z_1}(z_0, z_1 \mid s_1)\, dz_0 dz_1 = \int\limits_{-\infty}^{\infty} \int\limits_{z_1}^{\infty} p_{Z_1 Z_0}(z_0, z_1 \mid s_1)\, dz_0 dz_1. \quad (3.36)$$

Since, as Reference [10] shows, Z_0 and Z_1 are independent and are each non-negative, Equation 3.36 can be rewritten

$$P_{b|1} = \int\limits_{0}^{\infty} p_{Z_1}(z_1)\, dz_1 \int\limits_{z_1}^{\infty} p_{Z_0}(z_0)\, dz_0. \quad (3.37)$$

Evaluating the second integral results in

$$\int\limits_{z_1}^{\infty} p_{Z_0}(z_0)\, dz_0 = \int\limits_{z_1}^{\infty} \frac{1}{2\sigma^2} e^{-\frac{z_0}{2\sigma^2}} dz_0 = -e^{-\frac{z_0}{2\sigma^2}} \Big|_{z_1}^{\infty} = e^{-\frac{z_1}{2\sigma^2}}. \quad (3.38)$$

Next, substitute Equation 3.33 and the result of Equation 3.38 into Equation 3.37 as shown below,

$$P_{b|1} = \int\limits_{0}^{\infty} e^{-\frac{z_1}{2\sigma^2}} \cdot \frac{1}{2\sigma^2} e^{-\frac{\left(z_1 + 2A^2\right)}{2\sigma^2}} I_0\left(\frac{\sqrt{2A^2 z_1}}{\sigma^2}\right) dz_1 = \int\limits_{0}^{\infty} \frac{1}{2\sigma^2} e^{-\frac{\left(2z_1 + 2A^2\right)}{2\sigma^2}} I_0\left(\frac{\sqrt{2A^2 z_1}}{\sigma^2}\right) dz_1. \quad (3.39)$$

This integral can be evaluated [10] to obtain

$$P_{b|1} = \frac{1}{2} e^{-\frac{A^2}{2\sigma^2}}. \quad (3.40)$$

Assuming that each symbol is equally likely and, due to the symmetry of the receiver, the probability of bit error is

$$P_e = P_{b|1}P_1 + P_{b|0}P_0 = \frac{1}{2}\left(\frac{1}{2}e^{-\frac{A^2}{2\sigma^2}}\right) + \frac{1}{2}\left(\frac{1}{2}e^{-\frac{A^2}{2\sigma^2}}\right) = \frac{1}{2}e^{-\frac{A^2}{2\sigma^2}} \tag{3.41}$$

where $P_0 = P_1 = 1/2$ is the probability of each symbol transmission. Now substituting $\sigma^2 = N_0/T_b$ and expressing the energy per symbol as $E = A^2T_b$, the probability of bit error for a noncoherently detected BFSK signal corrupted by AWGN is

$$P_e = \frac{1}{2}e^{-\frac{E_b}{2N_0}}. \tag{3.42}$$

A plot of Equation 3.42 is shown in Figure 3.

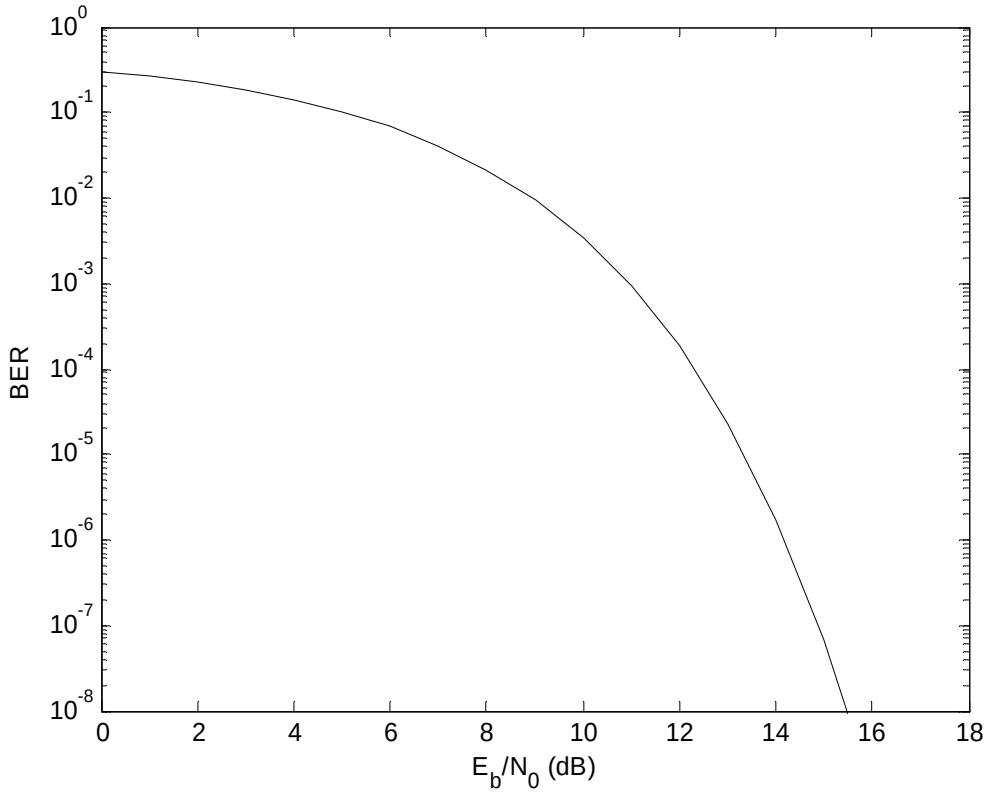

Figure 3. BER for Noncoherent BFSK in AWGN

2. Noncoherent Quadrature Receiver with Diversity

In order to combat the effects of interference and noise in a digital communications link, diversity can be employed. Diversity involves adding a level of redundancy to the transmitted bit stream by sending the same information multiple times [11]. One

straightforward way to achieve diversity is through the use of repetition coding. A repetition code is a $(n,1)$ linear block code where each data bit is transmitted n times, yielding two length n codewords, n 0's and n 1's. Based on the n diversity receptions, the receiver decides which bit was actually sent. This decision is made through either hard-decision or soft-decision demodulation [9].

A hard-decision receiver, also called majority vote, demodulates and decides which signal (code bit) was sent for each diversity reception. Figure 4 shows a diagram of a BFSK hard-decision receiver. The "choose largest" block compares $Z_{1k} \gtrless Z_{0k}$ and outputs a "1" on one output and a "0" on the other for each k^{th} diversity reception. A total of L comparisons are made for each codeword (i.e., for each data bit). The vote count for each signal branch is tallied by the summation operator and is represented by Z_1 and Z_0. This therefore implies that Z_1 and Z_0 take on integer values between 0 and L, with their sum equaling L. The "majority vote" block compares Z_1 to Z_0 and outputs a "1" decision if Z_1 is larger and a "0" if Z_0 is larger. If L is even, $Z_1 = Z_0$ is possible. In such a case either "0" or "1" maybe selected randomly.[9]

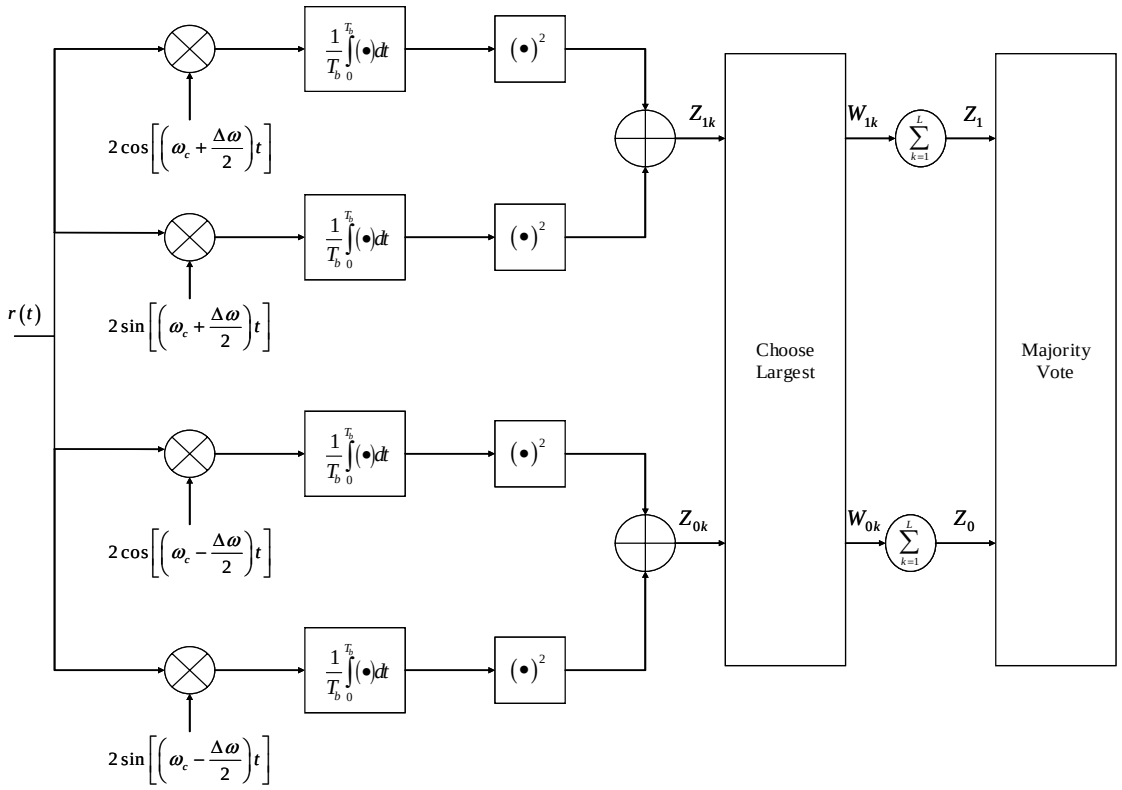

Figure 4. Noncoherent BFSK Hard-Decision Receiver (From [9].)

In contrast to hard-decision demodulation, a soft-decision receiver does not decide which signal (code bit) was sent for each diversity reception. Figure 5 shows a diagram of a BFSK soft-decision receiver. The receiver keeps a running total of the analog outputs of each dual branch as the diversity receptions are received. This total is represented as Z_1 and Z_0 but, unlike the hard-decision receiver, a decision as to whether a coded bit "1" or "0" was sent is not made at this point. After all diversity receptions are received, the 'choose largest' block compares Z_1 to Z_0 and decides that a "1" was transmitted if $Z_1 > Z_0$, and that a "0" was transmitted if $Z_1 < Z_0$. All total, there is only one decision per data bit made during the process. Compare this to hard-decision demodulation where a decision is made for each diversity reception and also in the majority vote count [9].

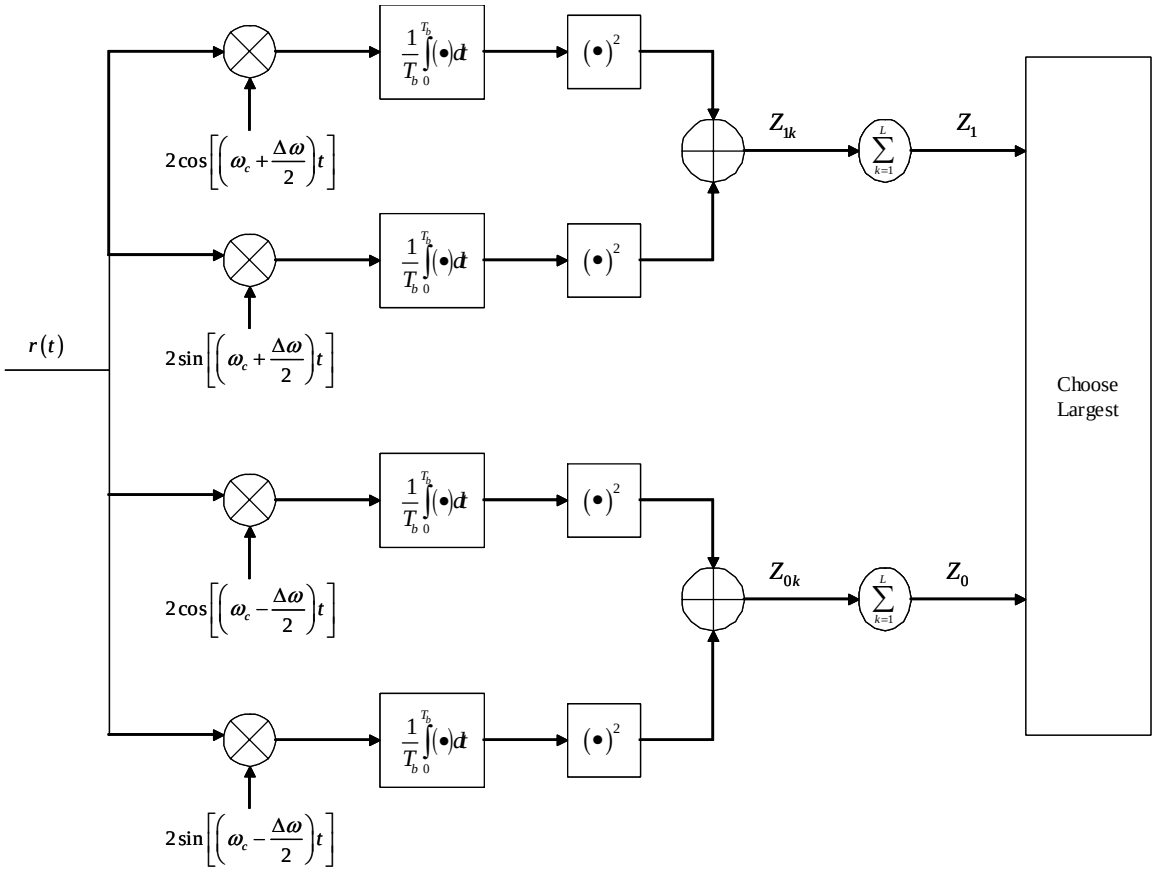

Figure 5. Noncoherent BFSK Soft-Decision Receiver (From [9].)

3. BER for Optimal Noncoherent Detection of BFSK in AWGN with Diversity and Hard-Decision Demodulation

The BER for BFSK in AWGN with repetition coding and hard-decision noncoherent demodulation is based on the result derived previously for noncoherently detected BFSK in AWGN without diversity. That result is repeated below, but now the energy-per-bit is the energy-per-code-bit, and the probability of error is the probability of code bit error,

$$P_e = \frac{1}{2} e^{-\frac{E_{b_c}}{2N_0}}. \tag{3.43}$$

As with the derivation in the no-diversity case, if we assume a "1" was sent, then W_{0k} in Figure 4 will be one with probability given by Equation 3.43 (i.e., when a code bit error

has occurred). Because it can take on only one of two values (0 or 1), W_{0k} is called a Bernoulli random variable. The process taking place in the hard-decision receiver is an example of a Bernoulli trial where the experiment has two possible outcomes and we are trying to determine the probability that an event (encoded bit error) is observed exactly i times out of L trials [12]. Following the procedures outlined in [13], and recalling that diversity receptions received in AWGN are independent [10], the probability that i of L diversity receptions will be received in error in a specific order is given by

$$\Pr\{i \text{ of } L \text{ diversity receptions received in error in a specific order}\} = p^i(1-p)^{L-i} \quad (3.44)$$

where p is the probability of diversity reception error ($W_{0k} = 1$) given by Equation 3.43 and $1-p$ is the probability of not making a diversity reception error ($W_{0k} = 0$).

The probability given by Equation 3.44 is for one ordered sequence of i errors and $L-i$ correct decisions. The binomial coefficient is the number of possible distinct sequences that have i errors and $L-i$ correct decisions, counting all orderings, and is given by [12]

$$\binom{L}{i} = \frac{L!}{i!(L-i)!}. \quad (3.45)$$

Therefore,

$$\Pr[i \text{ of } L \text{ diversity receptions received in error}] = \binom{L}{i} p^i (1-p)^{L-i}. \quad (3.46)$$

The receiver will make an error when more than half of the diversity receptions are in error. Therefore, we must take into account if L is even or odd. Combining Equations 3.44 and 3.45, the probability of error, given than L is odd, is the probability that $i \geq (L+1)/2$ and is given by

$$P_b(L) = \sum_{i=\frac{L+1}{2}}^{L} \binom{L}{i} p^i (1-p)^{L-i}. \quad (3.47)$$

When L is even, a coin is flipped for a tie and the probability of error is the probability that $i \geq (L/2)+1$ plus half the probability that $i = L/2$ and is given by

$$P_b(L) = \frac{1}{2}\binom{L}{L/2} p^{L/2}(1-p)^{L/2} + \sum_{i=\frac{L}{2}+1}^{L} \binom{L}{i} p^i (1-p)^{L-i}. \tag{3.48}$$

The bit error rates for different levels of diversity are shown in Figure 6 below. As the graph shows, increased diversity results in higher BER performance.

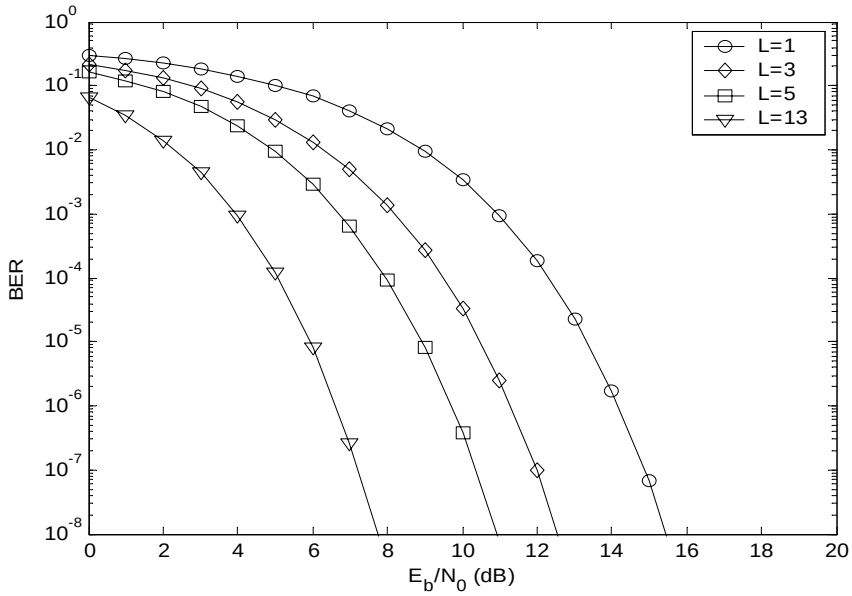

Figure 6. Noncoherent BFSK with Diversity and Hard-Decision Demodulation

4. BER for Optimal Noncoherent Detection of BFSK in AWGN with Diversity and Soft-Decision Demodulation

Following the procedure outlined in Reference [9], for the BER derivation with soft-decision demodulation, Equations 3.33 and 3.34 are modified slightly to take into account multiple diversity receptions. Thus, z_1 is replaced with z_{1_k} and z_0 is replaced with z_{0_k} to represent the k^{th} diversity reception. Equations 3.33 and 3.34 now become

$$p_{Z_{1_k}}\left(z_{1_k}\right) = \frac{1}{2\sigma^2} e^{-\frac{\left(z_{1_k}+2A^2\right)}{2\sigma^2}} I_0\left(\frac{\sqrt{2A^2 z_{1_k}}}{\sigma^2}\right) u\left(z_{1_k}\right) \tag{3.49}$$

and

$$p_{Z_{0_k}}\left(z_{0_k}\right)=\frac{1}{2\sigma^2}e^{-\frac{z_{0_k}}{2\sigma^2}}u\left(z_{0_k}\right) \tag{3.50}$$

where $\sigma^2 = N_0/T_c$. Recall that Equations 3.49 and 3.50 are the PDFs of chi squared random variables. Referring to Figure 5 and Reference [9], and recalling that each diversity reception is independent, then Z_1 and Z_0 are each the sum of independent random variables. Using the relationship that summing random variables corresponds to convolving their PDFs, and assuming that s_1 is transmitted with diversity L, the PDFs for Z_1 and Z_0 can be written as

$$\begin{aligned} p_{Z_1}\left(z_1 \mid s_1\right) &= p_{Z_{11}}\left(z_{11} \mid s_1\right) * p_{Z_{12}}\left(z_{12} \mid s_1\right) * \ldots * p_{Z_{1L}}\left(z_{1L} \mid s_1\right) \\ p_{Z_0}\left(z_0 \mid s_1\right) &= p_{Z_{01}}\left(z_{01} \mid s_1\right) * p_{Z_{02}}\left(z_{02} \mid s_1\right) * \ldots * p_{Z_{0L}}\left(z_{0L} \mid s_1\right) \end{aligned} \tag{3.51}$$

where $*$ denotes convolution. Next, utilizing the property that convolution in the time domain corresponds to multiplication in the Laplace domain, yields

$$\begin{aligned} \mathcal{L}\left\{p_{Z_1}\left(z_1 \mid s_1\right)\right\} &= \left[\mathcal{L}\left\{p_{Z_{1k}}\left(z_{1k} \mid s_1\right)\right\}\right]^L \\ \mathcal{L}\left\{p_{Z_0}\left(z_0 \mid s_1\right)\right\} &= \left[\mathcal{L}\left\{p_{Z_{0k}}\left(z_{0k} \mid s_1\right)\right\}\right]^L \end{aligned} \tag{3.52}$$

where $\mathcal{L}[\ ]$ denotes the Laplace Transform. From table lookup [9]

$$\begin{aligned} \mathcal{L}\left\{p_{Z_{1k}}\left(z_{1k} \mid s_1\right)\right\} &= \frac{1}{2\sigma^2}\left(\frac{1}{s+1/2\sigma^2}\right)e^{-\frac{A_c^2}{\sigma^2}\left(\frac{s}{s+1/2\sigma^2}\right)} \\ \mathcal{L}\left\{p_{Z_{0k}}\left(z_{0k} \mid s_1\right)\right\} &= \frac{1}{2\sigma^2}\frac{1}{s+1/2\sigma^2}. \end{aligned} \tag{3.53}$$

From the definition of the Laplace transform and Equations 3.51 thru 3.53, the PDFs can be written

$$\begin{aligned} p_{Z_1}\left(z_1 \mid s_1\right) &= \mathcal{L}^{-1}\left\{\left[\mathcal{L}\left\{p_{Z_{1k}}\left(z_{1k} \mid s_1\right)\right\}\right]^L\right\} \\ p_{Z_0}\left(z_0 \mid s_1\right) &= \mathcal{L}^{-1}\left\{\left[\mathcal{L}\left\{p_{Z_{0k}}\left(z_{0k} \mid s_1\right)\right\}\right]^L\right\} \end{aligned} \tag{3.54}$$

where $\mathcal{L}^{-1}[\ ]$ denotes the inverse Laplace transform. Again from table lookup [9], Equation 3.54 becomes

$$p_{Z_1}(z_1 \mid s_1) = \frac{z_1^{\frac{(L-1)}{2}}}{2\sigma^2 \left(2LA_c^2\right)^{\frac{(L-1)}{2}}} e^{-\frac{\left(z_1+2LA_c^2\right)}{2\sigma^2}} I_{L-1}\left(\frac{A_c\sqrt{2Lz_1}}{\sigma^2}\right) u(z_1)$$
$$p_{Z_0}(z_0 \mid s_1) = \frac{z_0^{L-1}}{\left(2\sigma^2\right)^L (L-1)!} e^{-\frac{z_0}{2\sigma^2}} u(z_0) \tag{3.55}$$

where $I_{L-1}(\cdot)$ is the modified Bessel function of the first kind and order $L-1$. Equation 3.55 represents the PDFs of Z_0 and Z_1, assuming L diversity receptions, and will be used to determine the decision statistic.

An error will occur in the receiver when $Z_1 < Z_0$ assuming that s_1 is sent. Using the joint distribution, this can be expressed as

$$P_b(L) = \Pr[Z_1 < Z_0] = \int_{-\infty}^{\infty} \int_{z_1}^{\infty} p_{z_0 z_1}(z_0 z_1 \mid s_1)\, dz_0 dz_1 \tag{3.56}$$

where the probability will be a function of the number of diversity receptions L. Again since Z_0 and Z_1 are independent as per Reference [10], the joint distribution in Equation 3.56 can be factored to give

$$P_b(L) = \int_0^{\infty} \int_{z_1}^{\infty} p_{Z_0}(z_0 \mid s_1)\, p_{Z_1}(z_1 \mid s_1)\, dz_0 dz_1 = \int_0^{\infty} p_{Z_1}(z_1 \mid s_1) \left(\int_{z_1}^{\infty} p_{Z_0}(z_0 \mid s_1)\, dz_0 \right) dz_1. \tag{3.57}$$

This equation can be evaluated to obtain [9]

$$P_b(L) = \frac{1}{2^{2L-1}} e^{-\frac{LE_c}{2N_0}} \sum_{n=0}^{L-1} c_n \left(\frac{LE_c}{2N_0}\right)^n \tag{3.58}$$

where

$$c_n = \frac{1}{n!} \sum_{m=0}^{L-1-n} \binom{2L-1}{m}, \text{ and}$$

$E_c = A_c^2 T_c$ is the average energy-per-diversity reception.

Figure 7 shows a comparison between the two demodulation types of noncoherent BFSK with diversity. As the figure shows, the soft-decision technique provides a gain in E_b/N_0 over the hard decision technique. For example, at $L = 5$ and a BER of 10^{-6}, the gain in E_b/N_0 is approximately 1.5 dB.

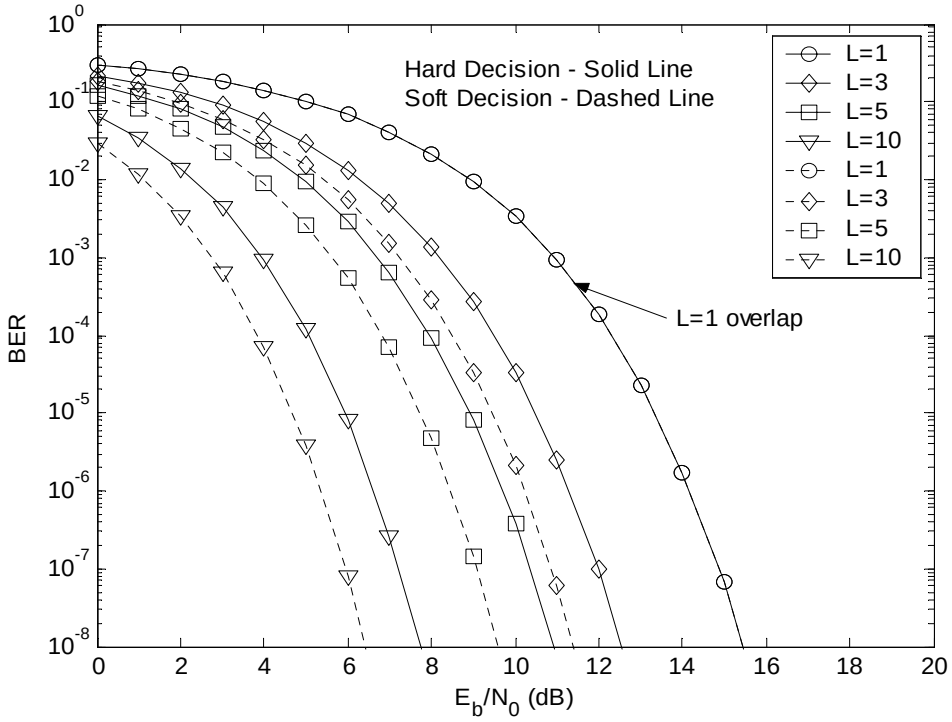

Figure 7. BER for Noncoherent BFSK with Diversity – Hard vs Soft Decision Demodulation

C. RICEAN CHANNEL

1. Fading Channels

Signals traveling in a mobile wireless communication system can take many routes to traverse the distance between the transmitter and the receiver. Objects in the path between transmitter and receiver can impede and reflect the signal causing multiple versions of the wave to arrive at the receiver at different times through different paths. This relates to the time dispersive characteristics of channels. Also, objects in the signal's path could be moving or the transmitter and receiver may be moving relative to

each other, thereby determining the time-varying nature of the channel. These combined effects cause fluctuations in the received signal's amplitude, phase, and frequency components. Such fluctuations are called multipath fading.[7]

a. Parameters

A number of parameters are used to describe a multipath channel. In order to describe the time dispersive nature of a channel, the delay spread and the coherence bandwidth are defined. The delay spread is found by observing the power out of the channel as a function of time delay and is often described in terms of its root-mean-square (rms) value. The coherence bandwidth is a measure of the maximum range of frequencies where signal amplitudes are highly correlated and is related to the delay spread. A measure of the amplitude correlation in terms of frequency is known as the frequency correlation function. If we assume the coherence bandwidth measures the range where the frequency correlation function is greater than 0.5, the following approximation can be used

$$B_c = \frac{1}{5\sigma_\tau} \tag{3.59}$$

where B_c is the coherence bandwidth and σ_τ is the rms delay spread [17].

While the coherence bandwidth and the delay spread describe the time dispersive nature of the channel, the coherence time and Doppler spread are used to describe its time-varying characteristics. As mentioned previously, Doppler shift is caused by the relative motion of the transmitter and receiver and is defined as

$$f_m = \frac{v}{\lambda} = v\frac{f}{c} \tag{3.60}$$

where v is relative speed, f is signal frequency, and c is the speed of light. Because different paths will experience different Doppler shift and because relative speed usually changes over time, this phenomenon causes a spreading of the received signal's spectrum. Doppler spread B_d measures the extent to which the spectrum is increased. The Doppler spread is a measure of the time-varying nature of the channel. The corresponding time-domain measure is the coherence time T_c. Coherence time measures the time

interval over which the channel effects on attenuation and phase are essentially constant. In other words, it is the time when amplitude correlation is high. For digital communications, a rule of thumb for the relationship between Doppler shift and coherence time is [17]

$$T_c = \frac{0.423}{f_m}. \tag{3.61}$$

b. Types of Fading

Given the characteristics of the channel, we can now define the different types of fading that a signal can experience. As related to the time dispersive nature of a channel, a signal can undergo either flat or frequency selective fading. Flat fading occurs when the channel response to the signal is constant attenuation and linear phase over the signal's entire bandwidth. In other words, the following relationships must hold;

$$B_s \ll B_c \text{ and } T_s \gg \sigma_\tau \tag{3.62}$$

where B_s is the bandwidth of the transmitted signal and T_s is the symbol period. If the above relationships do not hold, the channel is considered to be frequency selective. The time-varying nature of the channel determines whether it is classified as slow or fast fading. Slow fading describes a situation where the impulse response of the channel is changing slowly compared to the signal symbol duration. Similarly, the Doppler spread is much smaller than the signal bandwidth. These relationships are described as follows

$$T_s \ll T_c \text{ and } B_s \gg B_D. \tag{3.63}$$

As described in Reference [6], the symbol period should be less than the coherence time by a factor of 100 to 200 in order to avoid fast fading and the effects of errors induced by Doppler spread [7]. Conversely, fast fading occurs when the channel is changing faster than the transmitted signal and the Doppler spread is larger than the signal bandwidth [17].

c. Flat, Slow Fading Criteria

In order to relate coherence time and Doppler shift to a real-world system, we will assume that two VHF radios operating in the 30 to 88 MHz range over 25-kHz channels are communicating and one radio is in a vehicle traveling at 30 mph (13.41

m/s). Utilizing Equation 3.59, the maximum Doppler shift range can be calculated as follows

$$\begin{aligned} f_m &= v\frac{f}{c} = 13.41\,\text{m/s}\left[\frac{30\text{x}10^6\ \text{s}^{-1}}{3\text{x}10^8\ \text{m/s}}\right] = 1.34\ \text{Hz} \\ f_m &= v\frac{f}{c} = 13.41\,\text{m/s}\left[\frac{88\text{x}10^6\ \text{s}^{-1}}{3\text{x}10^8\ \text{m/s}}\right] = 3.93\ \text{Hz}. \end{aligned} \tag{3.64}$$

Next, using Equation 3.60, the coherence time can be found

$$\begin{aligned} T_c &= \frac{0.423}{f_m} = \frac{0.423}{1.34} = 316\ \text{ms} \\ T_c &= \frac{0.423}{f_m} = \frac{0.423}{3.93} = 108\ \text{ms}. \end{aligned} \tag{3.65}$$

From the above calculations, we see that, in order to satisfy slow fading and taking into account the criteria in Reference [6], the coherence time must be on the order of 100 to 200 times greater than the symbol duration and the signal bandwidth must be an order of magnitude greater than the Doppler spread. If we assume binary modulation, then the maximum bit period and minimum bit rate can be calculated as follows:

$$R_{b_{\min}} = (T_{b_{\max}})^{-1} = \left(\frac{T_c}{100}\right)^{-1} = \frac{100}{315\ \text{ms}} = 317\ \text{bps} \tag{3.66}$$

$$B_D = (3.93)\,\text{x}2 \approx 8\ \text{Hz} \ll B_s = 25\ \text{kHz}. \tag{3.67}$$

To analyze the flat fading case, we will assume $B_c = 250$ kHz which satisfies one of the flat fading constraints. Utilizing this assumption and Equation 3.58, the rms delay spread is

$$\sigma_\tau = \frac{1}{5B_c} = \frac{1}{5\left(250\text{x}10^3\ \text{Hz}\right)} = 800\ \text{ns}. \tag{3.68}$$

This seems reasonable because the corresponding difference in multipath lengths is $800\ \text{ns} \cdot 3\text{x}10^8\ \text{m/s} = 240$ meters. From Equation 3.61, the symbol period must be an or-

der of magnitude greater than the rms delay spread in order for the channel to be flat fading. This results in

$$R_{b_{\max}} = \left(T_{b_{\min}}\right)^{-1} = \left[10\left(\sigma_\tau\right)\right]^{-1} = \left(8\text{x}10^{-6}\right)^{-1} = 125 \text{ kbps.} \tag{3.69}$$

The above analysis demonstrates how characterizing the channel as flat places an upper limit on the symbol rate, whereas the slow fading criterion sets a lower limit on the symbol rate [7].

2. BER of Noncoherent BFSK over Frequency Non-Selective, Slowly Fading Ricean Channel

Power in the received signal is the result of either line-of-sight (LOS) or multipath. LOS refers to an unobstructed path the signal takes directly from the transmitter to the receiver. Because of the effects of multipath, the received signal amplitude is no longer constant but is instead a random variable. If there is LOS power but a significant amount of power is received by way of multipath, then the Ricean model can be used to describe the channel. With this model, the amplitude fluctuations of the received signal (the random variable) are described by the Ricean PDF. If all received power is from the reflected or scattered signal power (i.e., no LOS power is received), then the fading is called Rayleigh fading, which is a special case of Ricean fading [17].

In Section B of this chapter, the probability of bit error for noncoherent BFSK was derived for the case when the signal amplitude was constant. Here this is extended to consider the signal amplitude as a random variable and, therefore, include the effects of the fading channel. The goal is again to determine the probability of symbol (bit) error, given the random nature of the signal's amplitude. A passband signal can be represented as

$$s(t) = \sqrt{2}a_c \cos\left[2\pi f_i(t)t + \theta(t)\right] \tag{3.70}$$

where $E_s = a_c^2 T_s$ is the symbol energy. The probability of symbol error depends on the symbol energy, which in turn depends on the signal amplitude. But now the signal amplitude is random and thus the probabilities are conditional. Denoting $P_s(a_c)$ as the

probability of symbol error (as a function of a_c), the average probability of symbol error can be computed from the definition of the expected value as [7]

$$P_s = \int_0^\infty P_s(a_c)\, p_{A_c}(a_c)\, da_c \tag{3.71}$$

where $p_{A_c}(a_c)$ is the amplitude PDF. In order to relate the probability of symbol error to the energy, the following substitution is made [9]

$$\gamma_s = \frac{E_s}{N_0} = \frac{a_c^2 T_s}{N_0}. \tag{3.72}$$

Equation 3.59 can then be rewritten

$$P_s = \int_0^\infty P_s(\gamma_s)\, p_{\Gamma_s}(\gamma_s)\, d\gamma_s \tag{3.73}$$

where $p_{\Gamma_s}(\gamma_s)$ is the PDF of the ratio of the symbol energy to the noise power density.

Ricean and Rayleigh fading are considered. Referring back to Equation 3.59, if a_c is considered to be modeled as a Ricean random variable, its PDF can be written

$$p_{A_c}(a_c) = \frac{a_c}{\sigma^2} e^{\left[-\frac{\left(a_c^2+\alpha^2\right)}{2\sigma^2}\right]} I_0\left(\frac{\alpha a_c}{\sigma^2}\right) u(a_c). \tag{3.74}$$

Using the definition of the expected value and Equation 3.60, it can be shown the average received signal power is [9]

$$\overline{s^2(t)} = \overline{a_c^2} = \alpha^2 + 2\sigma^2. \tag{3.75}$$

As Reference [9] describes, α^2 and $2\sigma^2$ represent the LOS signal power and the multi-path signal power, respectively. The Rayleigh distribution is found by letting $\alpha = 0$ (no LOS) in Equations 3.74 and 3.75. This results in the following PDF:

$$p_{A_c}(a_c) = \frac{a_c}{\sigma^2} e^{-\frac{a_c^2}{2\sigma^2}} u(a_c). \tag{3.76}$$

The ratio of LOS power to diffuse (non LOS) power is often used to describe a channel and is given by

$$\varsigma = \frac{\alpha^2}{2\sigma^2}. \tag{3.77}$$

Referring back to Equation 3.73, in order to solve for the probability of symbol error, we still need to find the PDF $p_{\Gamma_s}(\gamma_s)$. Once this distribution is found, Equation 3.73 can be evaluated. This derivation is found in Reference [9], which also shows the end result for the performance of noncoherent BFSK over frequency non-selective, slowly fading Ricean channel (i.e., the solution of Equation 3.73). This is

$$P_b = \frac{1+\varsigma}{2(1+\varsigma)+\overline{\gamma_b}} e^{-\frac{\varsigma\overline{\gamma_b}}{2(1+\varsigma)+\overline{\gamma_b}}}. \tag{3.78}$$

For BFSK, the symbol energy is equal to the bit energy and this is represented in Equation 3.78 by substituting $\gamma_s = \gamma_b$. Because the received amplitude is random, the E_b/N_0 in Equation 3.78 represented by $\overline{\gamma_b}$ is an average. A graph of Equation 3.78 for different ratios of LOS to diffuse power is shown in Figure 8.

As the graph in Figure 8 shows, increasing the ratio of the LOS power to the diffuse power ς causes the curve to approach the AWGN channel case. This represents decreasing multipath power to a point where the LOS power is dominant and the effects of fading are negligible. On the other hand, the case when $\varsigma = 0$ represents Rayleigh fading. Here, there is no LOS power and the received signal power is completely from scattered paths.

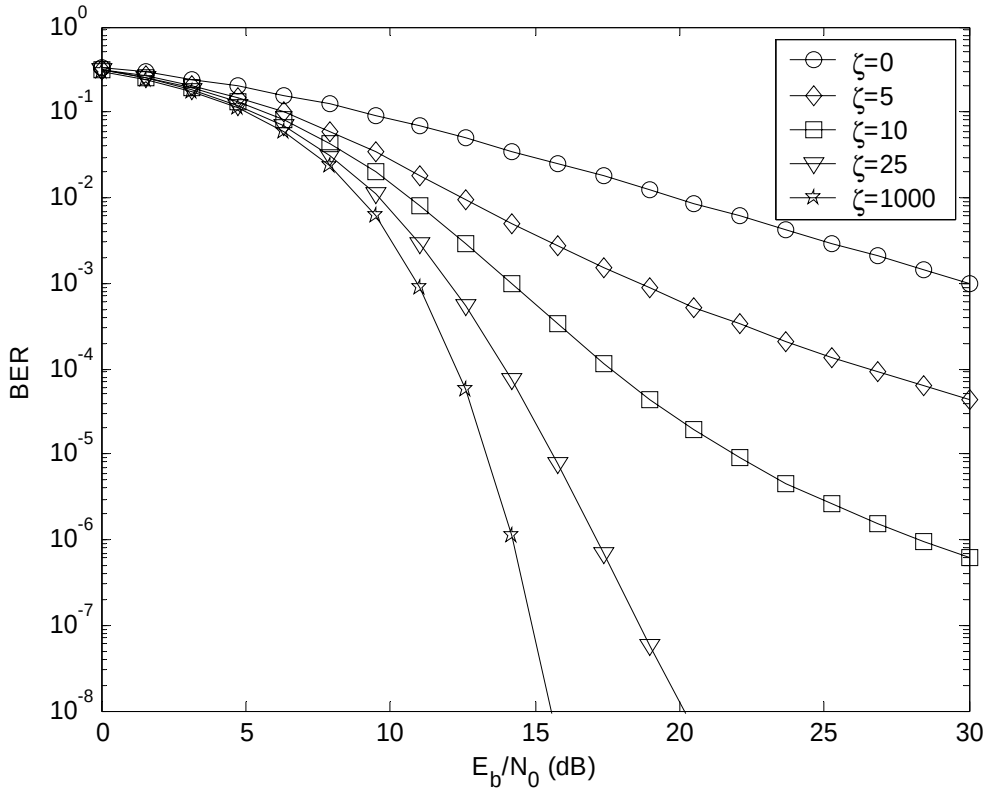

Figure 8. BER for Noncoherent BFSK in Frequency Non-Selective, Slow Fading Channel

This chapter analytically examined the performance of the SINCGARS for various channel assumptions and levels of diversity. The next chapter discusses a computer simulation of the SINCGARS physical layer and compares the simulation results with the results derived in this chapter.

IV. SIMULATION

This chapter discusses a computer model used to simulate the physical layer of the SINCGARS, modeled as a slow frequency-hopping, BFSK radio. Additionally, the simulation will consider the radio operating in the SINCGARS Data Mode (SDM) and transmitting at a bit rate of 16 kbps. As was discussed earlier in Chapter II 2, at this data rate the radio does not incorporate channel coding.

A. SIMULATION SETUP

The simulation of the physical layer was done using MATLAB version 7.0.1 and Simulink version 6.1. A block diagram of the Simulink model is shown in Figure 9.

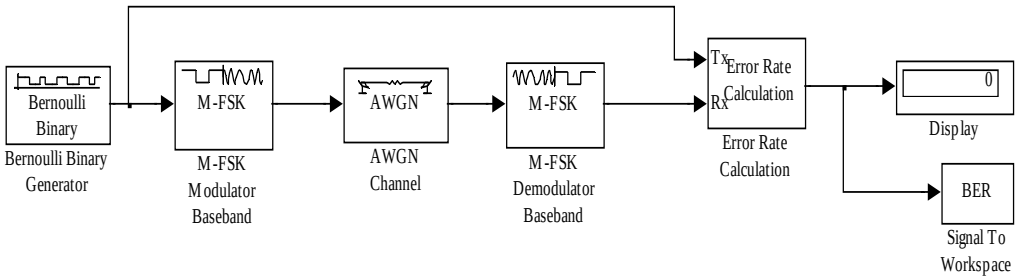

Figure 9. Simulink Model BFSK System in AWGN

The Simulink blocks *M*-FSK Modulator and *M*-FSK Demodulator use the equivalent lowpass representation of the FSK signal to modulate and demodulate the binary data. The results obtained from this simulation can be extended to the passband case since the BER analysis is independent of the carrier frequency. For this analysis, $M = 2$ is used to represent a BFSK system and the symbols were separated in frequency by the bit rate ($16\,\text{kHz}$). As discussed in Chapter III, this frequency separation will ensure orthogonal signaling. The Bernoulli Binary Generator outputs random ones and zeros to represent the data. Simulink assigns the higher frequency to the zero and the lower frequency to the one. A description of each block in the model is provided in Table 2 [14].

Bernoulli Binary Generator	Generates random bits with a Bernoulli Distribution. Outputs a "0" with probability p and a "1" with probability $1-p$.
M-FSK Modulator Baseband	Modulates the binary data with a baseband representation of an FSK signal ($M = 2$ for BFSK)
AWGN Channel	Adds white noise to the input signal.
M-FSK Demodulator Baseband	Demodulates the baseband representation of the FSK signal.
Error Rate Calculation	Compares the transmitted signal with the signal received after demodulation and calculates the error rate.
Signal To Workspace	Stores the information computed in the error rate block for use in the MATLAB workspace.
Display	Displays the running statistics of the error rate calculation block.

Table 2. Simulink Model Block Description

1. Monte Carlo Method

Bit (or symbol) error rates can be estimated from a simulation by comparing the received bit stream to the bit stream generated by the data source and counting discrepancies. This is the basis of the Monte Carlo Method. Given that N_b bits were received and n_e errors detected, the BER is estimated as

$$P_b = \frac{n_e}{N_b}. \tag{4.1}$$

If the same simulation was run again, a different realization of the AWGN would cause the estimated BER, in general, to be different from the first. This is because the noise is random and thus the detected number of errors is a random variable. The Strong Law of Large Numbers dictates that the average number of detected errors will approach a number $\bar{n}$ as the number of simulations is increased [12]. Therefore, the true BER can be expressed as

$$P_b = \frac{\bar{n}}{N_b}. \tag{4.2}$$

This estimate of the error ratio is called unbiased [16].

Because the simulation involves only a finite number of bits, the value of $\bar{n}$ is not known precisely, but it is estimated, to include a measure of confidence in the estimate. The probability that $\bar{n}$ will fall within a range is called the confidence level and can be expressed as

$$\Pr\left[n_L \le \bar{n} \le n_U \mid n_e, N_b\right] = \Theta \qquad 0 \le \Theta \le 1 \tag{4.3}$$

where Θ is the confidence level, and n_L and n_U are the upper and lower limits, respectively. It can be shown that for a confidence level of 0.954 and under certain assumptions (effects of disturbances independent for each error, Gaussian distributed error count, $N_b \gg 1$, $n_e \ll N_b$), the length of the confidence interval ($n_L - n_U$) decreases as the number of errors n_e increases and is independent of N_b as long as N_b is large [16].

B. SIMULATION RESULTS

1. AWGN Channel

The Bit Error Rate Analysis Tool (BERTool) in MATLAB version 7.0 was used to run a Monte Carlo simulation utilizing the model in Figure 9. This graphical user interface links to the Simulink model and is able to control the simulation parameters, collect the BER data, and display the results in graphical form. Along with running Monte Carlo simulations, the BERTool function can also generate data and plot theoretical BER curves for various modulation schemes [15]. The simulation was run for E_b/N_0 values in increments of 1 dB and halted at each step when the total number of errors reached 100. From Reference [16], at 100 errors and a confidence level of 0.954, the ratio $n_U/n_L = 1.5$.

The results of the simulation are shown in Figure 10. The theoretical plot of coherent BFSK is displayed only to contrast the simulation results and to show that the *M*-FSK block in Simulink does use noncoherent reception. As the graph shows, the simulation results compare well with the theoretical results.

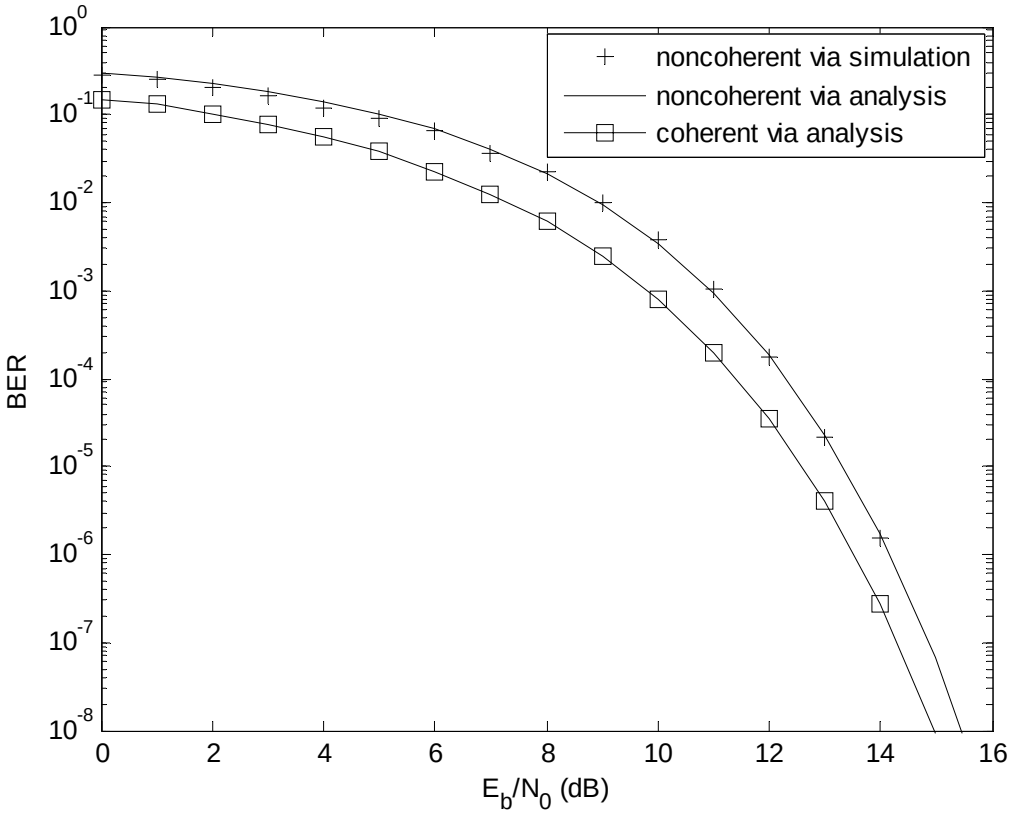

Figure 10. BER for BFSK in AWGN Channel via Simulation and Analysis

2. Ricean Channel

The simulation setup for noncoherent BFSK in a Ricean fading channel was identical to the setup shown in Figure 9 with the addition of the Ricean Fading Channel block. Two main parameters are used to determine how Simulink models the Ricean Channel. The first is a *K*-factor parameter which defines the ratio of LOS power to diffuse power. Recall from Chapter III that the Ricean channel models a system where there is a dominant LOS path but a significant amount of power at the receiver comes from non-LOS components. Thus, as $K \to \infty$ all the power is in the LOS path and the channel approaches the unfaded AWGN channel. The second main parameter is the maximum Doppler shift. Referring back to Chapter III, the Doppler shift is inversely proportional to the coherence time. For the simulation, the criteria that $T_c = 100T_s$ was used to ensure slow fading and which, along with a bit rate of 16 kbps and using Equation 3.61, provided for a maximum Doppler shift calculated as:

$$T_c = 100T_s = \frac{0.423}{f_m}$$
$$f_m = \frac{0.423}{100(1/16000)} \approx 68 \text{ Hz.} \tag{4.4}$$

From the above criteria, 100 bits are transmitted during the coherence time. Unlike the case for AWGN, there is a correlation within the coherence time window as to how the channel affects each bit (constant amplitude and phase over T_c). Therefore, a greater number of errors needed to be generated in order to take into account periods of varying degrees of fading. For this simulation, a limit of 2000 errors was used for the $K = 0,\ 5,$ and 10 case. In other words, at each E_b/N_0 value, the simulation was run until 2000 errors were generated. For the $K = 1000$ case (simulating $K \to \infty$ and AWGN), a large number of bits would need to be transmitted to generate a few errors at the higher E_b/N_0. Therefore, the simulation was run only up to 14 dB and stopped when the number of bits transmitted reached 50 million. Theoretically, this would produce approximately 50 errors. The results are shown in Figure 11 and, as the graphs show, the simulated results agree well with the theoretical.

This chapter discussed the physical layer simulation of the SINCGARS and compared the results with those derived in Chapter III. The next chapter describes a laboratory experiment where BER performance data was collected and presents the results.

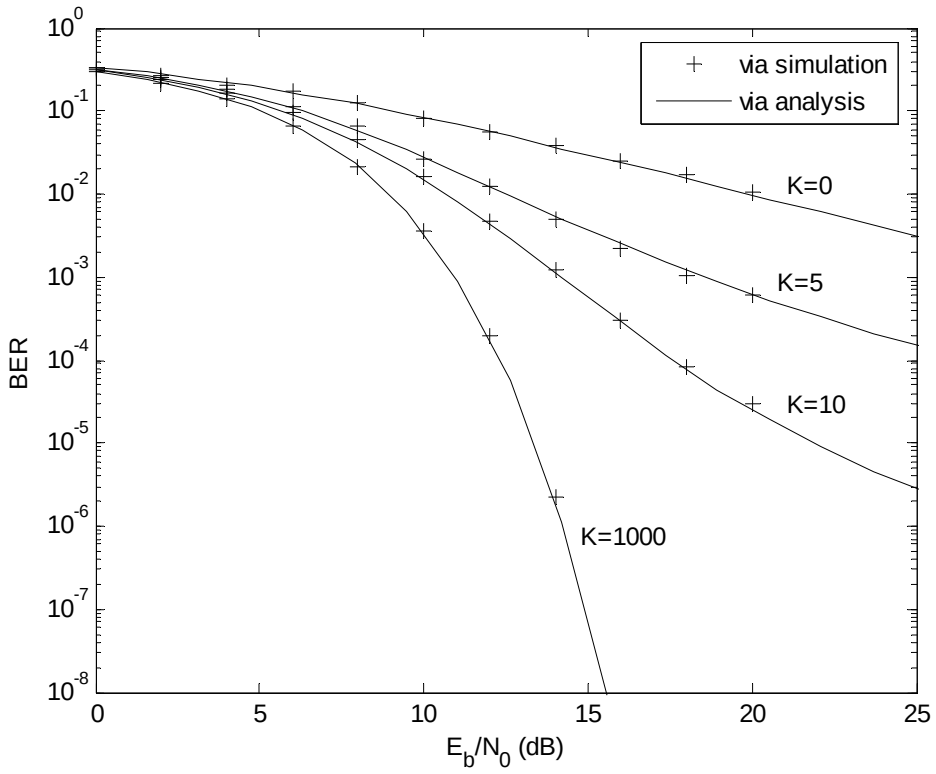

Figure 11. BER for Noncoherent BFSK in Ricean Channel via Simulation and Analysis

V. EXPERIMENTAL RESULTS

This chapter presents the results of a laboratory experiment to determine the BER performance of a SINCGARS operating in the SDR mode in an AWGN channel. The objective of the experiment was to measure the BER experienced by a SINCGARS receiver subjected to various amounts of AWGN with no fading. These results were later compared to the expected BERs, determined in earlier chapters via analysis and simulation, to determine how well the actual SINCGARS performance compares to optimum performance. The experiment was performed at the Marine Corps Tactical Systems Support Activity (MCTSSA) at Camp Pendleton, California. A block diagram showing a general overview of the experimental concept is shown in Figure 12.

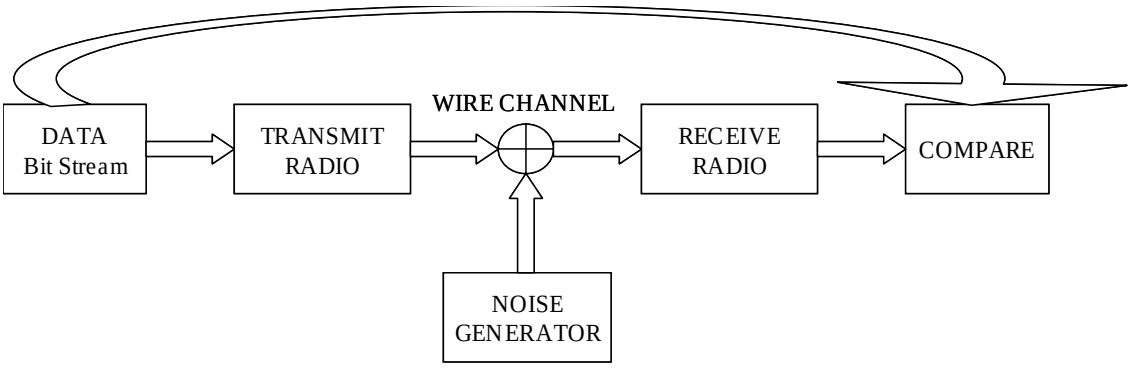

Figure 12. Experiment Overview

A. LABORATORY SETUP

The laboratory setup used in this experiment, including the probability-of-error application used to generate and collect data, was developed by MCTSSA. Two SINCGARS SIP radios operating in the SDR mode and transmitting at 16 kbps served as the test bed. Below is a description of the main components used in the experiment, including an overview of the probability of error application. For a more detailed description of this application, refer to Reference [18].

1. Main Components

Figure 13 is a diagram of the laboratory setup with the main components labeled. Refer to Reference [18] for more details on the individual components.

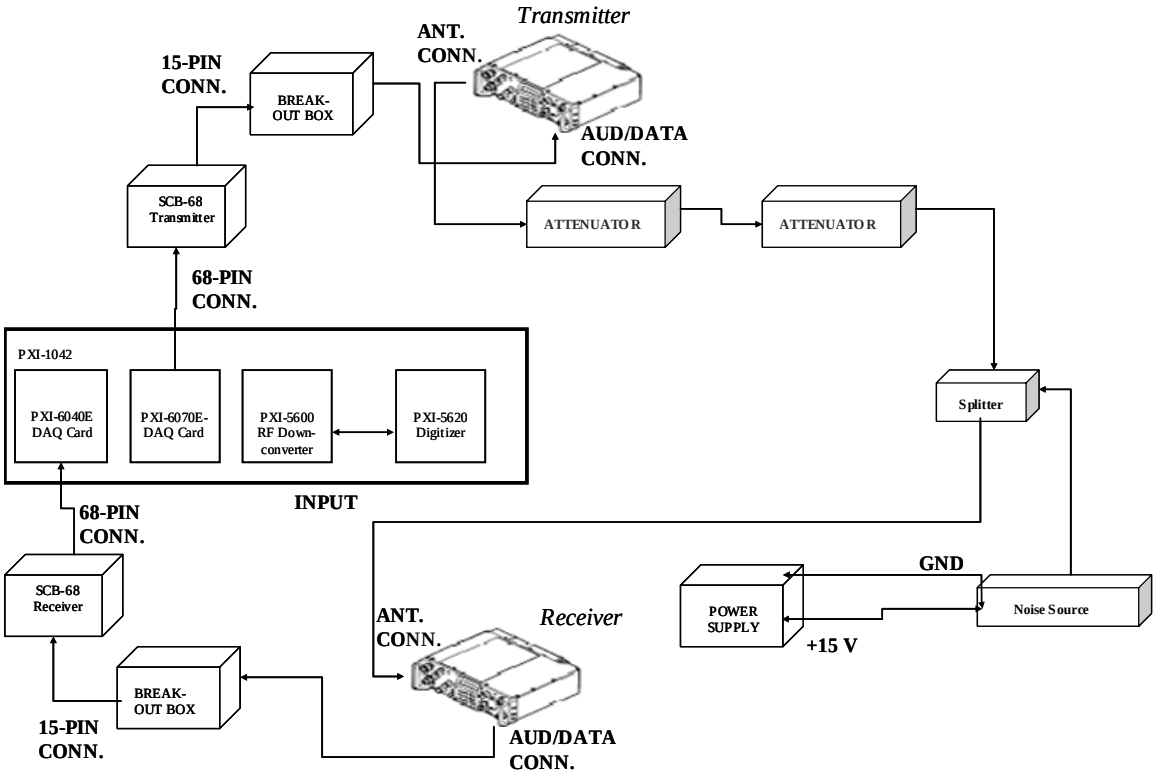

Figure 13. Laboratory Setup – Block Diagram [18]

PXI-1042: This general-purpose 8-slot chassis houses the multifunction Data Acquisition Devices (DAQ) and the PXI controller. Similar to a computer with peripheral slots, PXI modules can be added to the PXI-1042 to perform various PC based test and measurement functions.

SCB-68: This is a Shielded Input/Output Connector Block used to route signals to the 68-pin DAQ boards.

Break-Out Box: This box routes the signals from a 15-pin configuration to the appropriate SINCGARS input configuration.

Attenuators: This hardware attenuates the transmitted signal.

Splitter: The splitter combines the signal from the noise generator with the attenuated transmitted signal.

Noise Generator: This device is a voltage-controlled noise generator.

The probability-of-error application developed at MCTSSA utilizes LabVIEW to interface with the accompanying PC-based test and measurement hardware. This application serves as the software interface to the measurement hardware and is used to generate the data (bit stream) and to analyze the results. The transmitted data was created in LabVIEW as a random nonreturn-to-zero (NRZ) bit stream. The PC-based test and measurement hardware provides the capability to control and acquire data. The application allows the user to input the length of the data and also provides for text file output that shows the results of the experiment (i.e., number of bits sent/received, errors detected) [18]. Refer to Figures 14 through 19 for pictures of the laboratory setup.

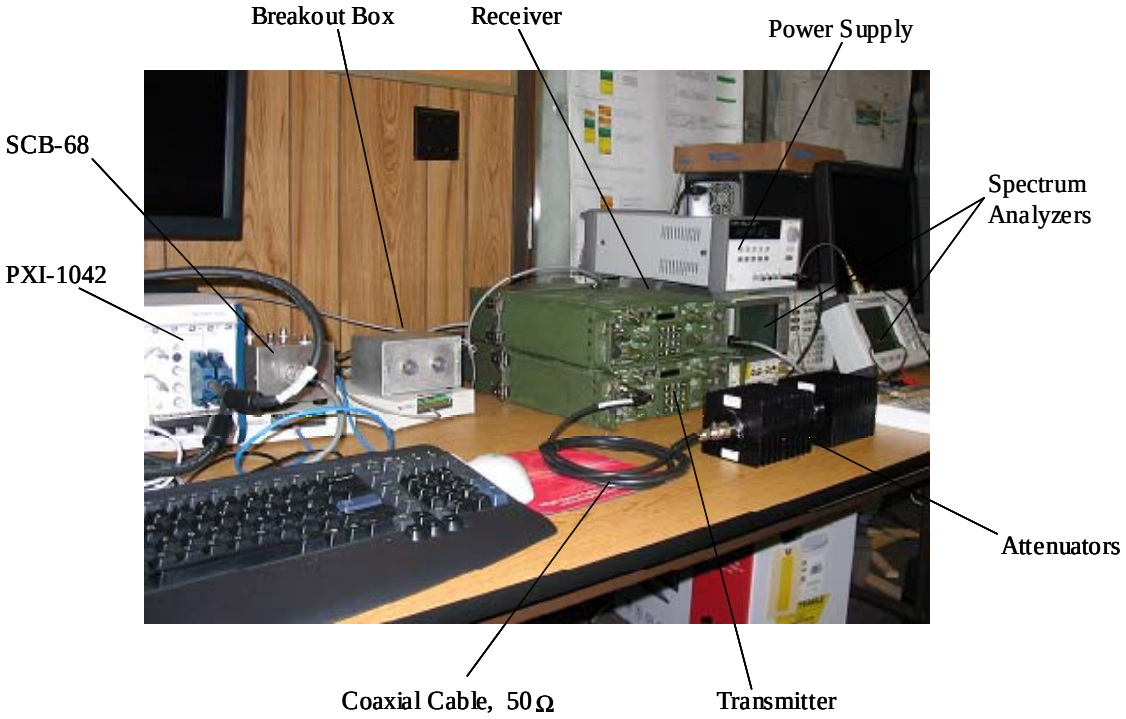

Figure 14. Laboratory Setup - Photo

Figure 15. PXI-1042

Figure 16. SCB-68 and Break-Out Box

Figure 17. Attenuators

Figure 18. SINCGARS

Figure 19. Noise Generator

B. LABORATORY PROCEDURE

Two separate data collection trials were performed using nearly the same basic laboratory setup. The first experiment, herein referred to as experiment A, was performed with the assistance of Capt. Max Green USMC, Capt. Juan Svenningsen USMC, and Nancy Ho of MCTSSA. A slightly modified trial, subsequently referred to as experiment B, was performed later by Capt Max Green and Nancy Ho. Procedures for each experiment are described in the following sections.

1. Experiment A

For experiment A, the signal and noise measurements were taken using an Anritsu SiteMaster S332D spectrum analyzer. Also, the following relationship was used;

$$\frac{E_b}{N_0} = \frac{P_r T_b}{N/W} = \frac{P_r / R_b}{N/W} \tag{5.1}$$

where P_r is the measured received signal power, N is the measured noise power, and W is the bandwidth. This relationship is used to convert between signal and noise power measurements and the E_b/N_0 values needed for comparisons with the analytical and simulation results. The signal power and/or noise power required adjustment in order to generate the correct range of values of E_b/N_0. With the radio in the low-power setting and using the radio's specifications, the expected power level out of the transmitter in Figure 13 is 0.5 mW or -3.0 dBm, where dBm is defined as

$$y(\text{dBm}) = 10\log_{10}\left(\frac{x}{1\text{ mW}}\right). \tag{5.2}$$

Next, the maximum generated noise power spectral density was measured at the output of the noise generator and found to be -111 dBm/Hz. Therefore, because of the limitations of the noise source, it was necessary to attenuate the transmitted signal. Due to the constraints of available equipment, the signal could only be attenuated to a level of -64.5 dBm, which, using the maximum available noise power spectral density, corresponded to a minimum measurable E_b/N_0 value of 4.46 dB. This calculation is

$$\frac{E_b}{N_0}(\text{dB}) = 10\log_{10}\left[\frac{P_r/R_b}{N_0}\right] = 10\log_{10}\left[\frac{10^{(-6.45)}\text{ mW}}{(16\text{x}10^3\text{ bps})10^{(-11.1)}\text{ mW/Hz}}\right] = 4.46\text{ dB}. \tag{5.3}$$

Note in Equation 5.3 that the measured signal power and noise power per hertz are usually given in dBm and must be converted using the relationship in Equation 5.2.

Trials were performed at various levels of signal-to-noise power. The signal power was first measured at the output of the splitter (prior to entering the receiver) with the voltage-controlled noise generator turned off and a bit stream of 1s transmitted. Then, with the radio off, a voltage was applied to the noise generator and a measurement again taken at the input of the receiver. From these two measurements and using Equations 5.2 and 5.3, an E_b/N_0 value could be obtained. Next, the probability of error application was run with the radio in the single channel (no frequency hopping) SDR mode and transmitting 16 kbps at a frequency of 71 MHz. After adjusting the noise generator

to obtain a new E_b/N_0, this process was repeated. Table 3 shows the number of bits transmitted and the number of errors received at each data collection point.

E_b/N_0 (dB)	4.46	4.71	6.46	8.46	10.94	13.46	15.96
Megabits transmitted	0.7	2.5	1.0	1.0	2.0	2.5	8.0
Bit errors detected	93,339	311,444	71,168	21,708	3547	409	59

Table 3. Experiment A Results

2. Experiment B

Experiment B utilized the same basic setup and procedure as experiment A, but instead of using an external spectrum analyzer to take power measurements, it used PC-based test and measurement hardware. Referring to Figure 13, an RF downconverter card and a digitizer card, both internal to the PXI-1042, were used to collect the information needed for the software to perform power and spectral analysis. The signal and noise power measurements were taken at the same points in the laboratory setup as in experiment A. Also, 22 data points were collected during experiment B. The results for both experiments are provided in the next section.

C. LABORATORY RESULTS AND DISCUSSION

1. Experiment A and B Results

The results from experiment A are shown in Figure 20 where the seven data points are plotted along with the analytical BER curve for an optimal noncoherent BFSK receiver in AWGN.

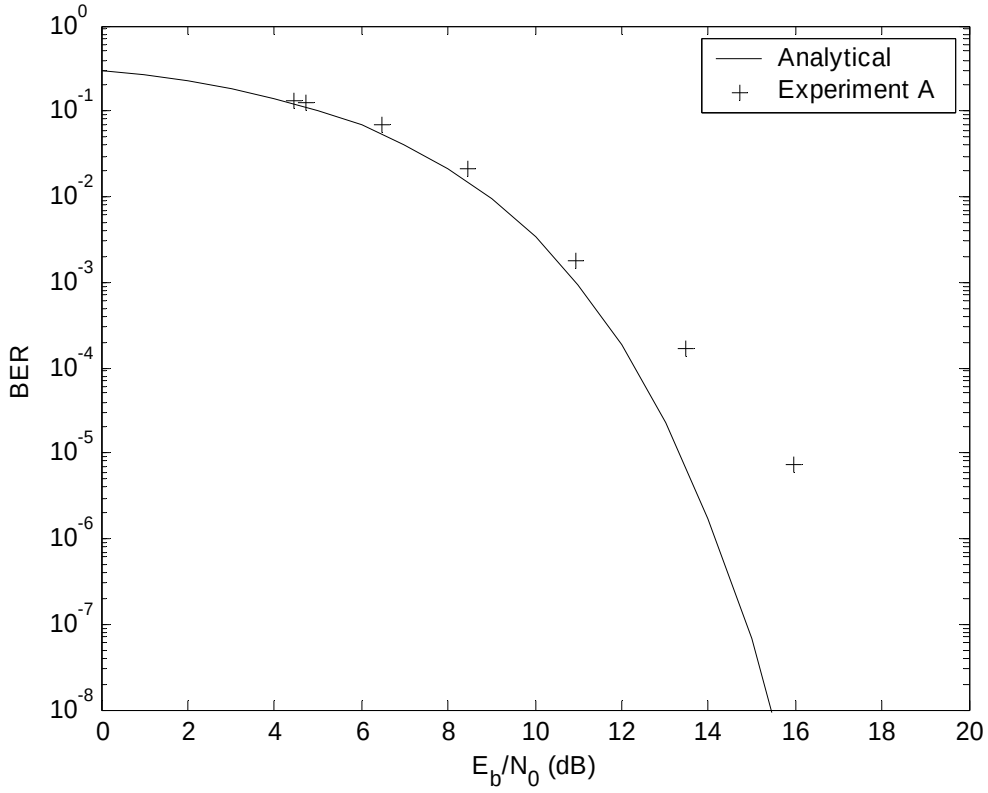

Figure 20. Experiment A Results

The plot reveals a deviation of the experimental results with the theoretical, and the deviation increases with increasing E_b/N_0. Figure 21 illustrates this deviation and shows the difference in dB between the expected and experimental E_b/N_0 for each BER.

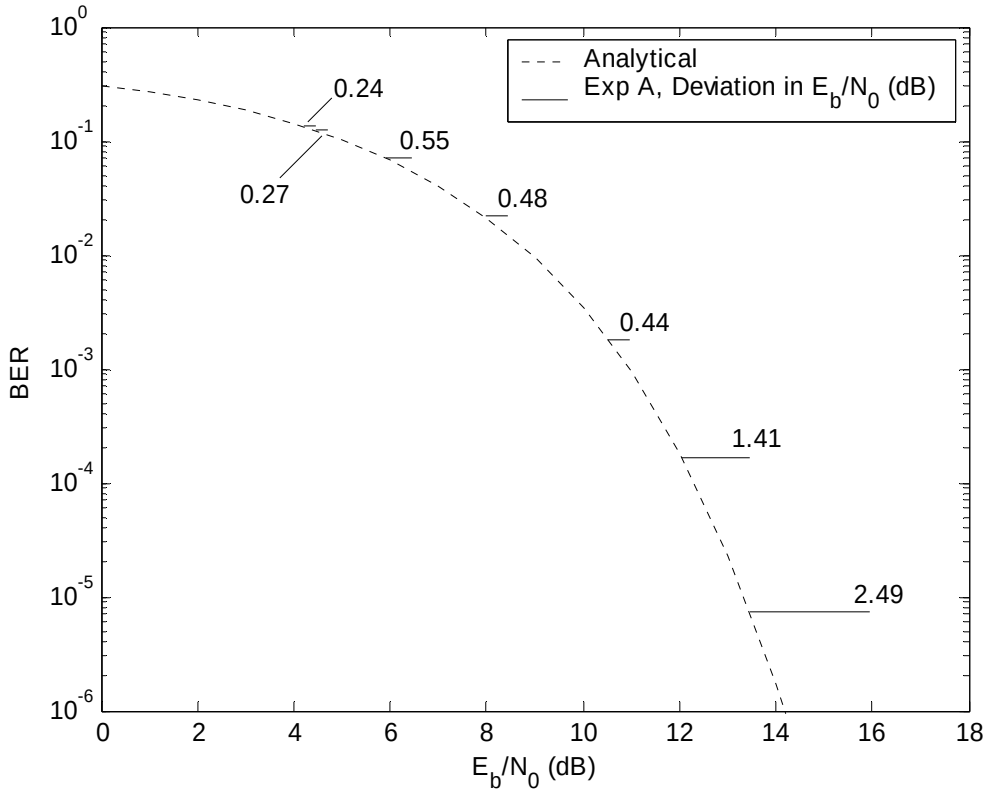

Figure 21. Experiment A Results: Deviation from Analytical

The results for experiment B are shown in Figure 22. For comparison, the results of experiment A are also plotted on the same graph along with the analytical BER curve. Again, note the deviation from analytical taking place at the higher values of E_b/N_0 in the experiment B results. In contrast, the data points for E_b/N_0 below 8 dB show performance better than optimal. These points will be addressed in the next section.

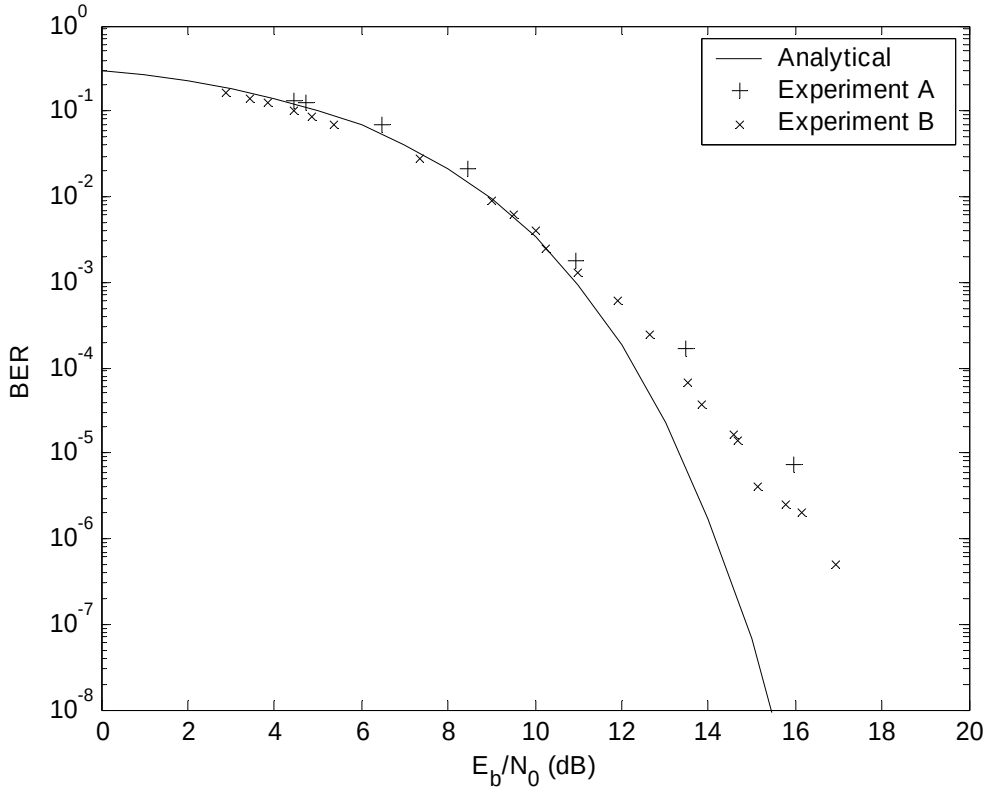

Figure 22. Experiment A and B Results Comparison

2. Discussion

Although the results of experiment A and B are slightly different, they both suggest the same trend. That trend is near optimal BER performance at lower E_b/N_0 values and an increasing deviation at the higher values. Additionally, the experiment B results suggest better-than-optimal radio performance for $E_b/N_0 < 8$ dB. Of course, actual BER performance can not be, on average, better-than-optimum BER performance. One possible explanation for this measured better-than-optimal performance is either the signal or noise power were measured incorrectly and the error was consistent throughout the experiment. If an underestimate of E_b/N_0 was the cause of super-optimum performance measurements, then that underestimate must have been at least 0.75 dB because the left-most seven points in Figure 22 were super-optimal by 0.75 dB. Correcting for this conjectured underestimate would result in a shift in the experimental data points to the right 0.75 dB. The new plot, with this correction, is shown in Figure 23.

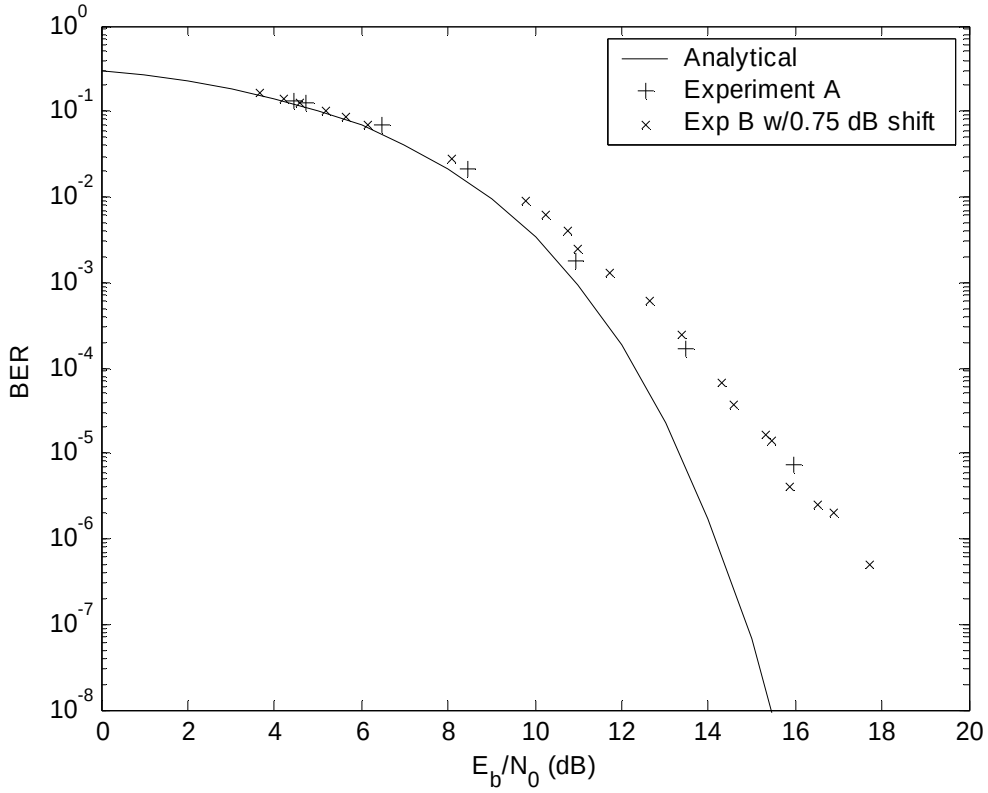

Figure 23. Comparison of Experimental Results – Experiment B Results Adjusted

The increasing sub-optimal performance at increasing values of E_b/N_0 described by both experiments may suggest flaws in the operation of the radio that are unmasked as the noise power weakens. In other words, a few errors inherent to the radio's operation would not be appreciably noticed at the stronger noise levels (lower E_b/N_0) where many errors are already being produced. This can be illustrated using the data from experiment A. Referring to Table 3, at 13.46 dB there were 409 errors received and the experimental BER was found to be $1.64\text{x}10^{-4}$. The theoretical BER at this E_b/N_0 can be calculated from Equation 3.42 as

$$P_b = \frac{1}{2}e^{-\frac{E_b}{2N_0}} = \frac{1}{2}e^{-\frac{1}{2}\left(10^{1.346}\right)} = 7.62\text{x}10^{-6}. \tag{5.4}$$

Therefore, for the 2.5 Mbits transmitted, we would theoretically expect approximately 19 errors. This is 390 errors less than the experimental result. If we assume the 390 errors

are due to flaws in the radio, they would likely also be present at the lower E_b/N_0 values. Again, referring to Table 3, experimentally at 4.71 dB and 2.5 Mbits transmitted, 311,444 errors were detected. Using Equation 5.4, theoretically we would expect 284,830 errors for 2.5 Mbits transmitted. Thus, 390 errors would easily be disguised within the thousands of errors detected and the change in BER would be negligible.

Aside from laboratory signal and noise power measurement errors, errant data would result if the probability of error application was not functioning properly. Incorrect timing or synchronization could cause the received bit stream to be 'off' by a number of bits, thus creating a much larger than expected number of errors. With this in mind, the application was first tested a number of times with the noise generator taken out of the setup. This resulted in zero received errors and thus provided a certain level of confidence that the application was functioning properly. As the experiment proceeded, we did find that occasionally a trial run would produce an unexpectedly large number of errors. Although the specific problem with these certain trials was not discovered, speculation is that the application encountered timing or synchronization problems. Therefore, the data from all trial runs where the received errors deviated dramatically from the expected number (and from the other similar trials) were discarded and not included in the BER calculation.

a. Performance and Range

The effects of sub-optimal performance at large SNR can also be examined in terms of the radio's range. All else constant, as the distance between the transmitter and receiver increases, the received power decreases [7]. Additionally, a radio operating sub-optimally will require a larger E_b/N_0 to achieve the same BER as a radio operating optimally. Therefore, for the same transmitted power, sub-optimal performance will have a negative effect on a radio's range as compared to optimal performance. To show this, we will use the results of experiment A and compare this with the results of an optimally performing radio.

From Table 3 and Figure 21, for a BER of $7.375\text{x}10^{-6}$, the difference between theoretical and experimental is 2.49 dB. In other words, to achieve the same BER,

a SINCGARS would require 2.49 dB more E_b/N_0 than the equivalent optimum noncoherent receiver. For this simple comparison, assume a free-space channel, an isotropic receive antenna, and equal antenna gains. Receiver "1" is operating sub-optimally and receiver "2" is optimal. From the definition of power

$$P_{r_1} = \left(\frac{E_b}{N_0}\right)_1 N_0 R_b \qquad P_{r_2} = \left(\frac{E_b}{N_0}\right)_2 N_0 R_b \tag{5.5}$$

where R_b is the bit rate and P_r is the receive power. As per Reference [7], the relationship between transmit and receive power utilizing the above assumptions is

$$P_r = \frac{P_t G_t G_r}{L_c} \tag{5.6}$$

where

P_t is the transmit power,

G_t and G_r are the transmit and receive antenna gains respectively, and

L_c is the channel loss.

The channel loss is related to the distance d between the transmitter and receiver by the equation

$$L_c = \left(\frac{4\pi df}{c}\right)^2 \tag{5.7}$$

where f is the operating frequency and c is the speed of light [7]. Substituting Equation 5.7 into 5.6 and defining d_1 and d_2 as the distance required to achieve the specified BER yields

$$P_{r_1} = P_t G_t G_r \left(\frac{c}{4\pi d_1 f}\right)^2 \qquad P_{r_2} = P_t G_t G_r \left(\frac{c}{4\pi d_2 f}\right)^2. \tag{5.8}$$

Assuming that the transmit power, the frequency, and the antenna gains are the same for both cases and taking the ratio of receive powers in Equation 5.8 results in

$$\frac{P_{r_2}}{P_{r_1}} = \frac{{d_1}^2}{{d_2}^2} \tag{5.9}$$

Substituting Equation 5.5 into Equation 5.9 and using the data from experiment A yields

$$\frac{d_1}{d_2} = \sqrt{\frac{P_{r_2}}{P_{r_1}}} = \sqrt{\frac{\left(E_b / N_0\right)_2}{\left(E_b / N_0\right)_1}} = \sqrt{10^{-2.49/10}} = 0.751. \tag{5.10}$$

This result shows that the sub-optimal performance results in approximately a 25% decrease in the radio's range when assuming a free-space channel. Extending these results to a fading channel, the conjecture is that sub-optimal performance in this environment would also cause a similar decrease in the radio's range.

This chapter presented the laboratory setup and experimental results. It also compared these results with the results obtained in Chapters III and IV. The next chapter presents the conclusions of this research and recommendations for future work.

VI. CONCLUSION AND FUTURE WORKS

A. CONCLUSION

This thesis examined the physical layer of the SINCGARS. This was done by modeling the radio as an optimal noncoherent BFSK system with no frequency-hopping, considering only the SDR mode of operation. The theoretical BER performance was derived for hard and soft decision demodulation and for different channel conditions. A computer simulation was conducted and compared with the theoretical results. Finally, an experiment was performed in the laboratory involving two radios transmitting and receiving data over a wire channel with AWGN. These results were compared with the results of a similar experiment and also with the theoretical and simulation results.

Although the simulation results agreed quite well with the theoretical, the experimental results showed an increasing deviation from the theoretical and simulation results for increasing values of E_b/N_0. Assuming no measurement errors, this suggests the radio is performing at a sub-optimal level and possibly explains why SINCGARS data communications performance is disappointing. This effect could easily be overlooked during voice transmission because of the less stringent BER requirement for acceptable reception. On the other hand, for data transmission, the presence of a relatively small number of errors could cause error rates that are not acceptable. Therefore, if the sub-optimal performance of the actual SINCGARS is corrected, data communications via SINCGARS would be improved. Results herein indicate that the required hardware changes for this improvement are in the receiver only. This change, therefore, would not change the waveform, and therefore, would be reverse compatible with the current SINCGARS. Since the need for data communications at the tactical level is growing substantially due to Network Centric Operations, improvement of data communications is a very real need for the SINCGARS and could possibly be addressed through these receiver hardware improvements that would bring the radio's performance closer to optimal levels.

B. FUTURE WORK

This thesis covers the simulation and analysis for fading channels, but contains experimental data for the unfaded AWGN channel only. The logical next step to complete the characterization of the physical layer would be to devise an experiment similar to the one in this thesis but modified to operate in the more realistic outdoor wireless environment. This step is necessary to ascertain if the suboptimal performance measured in the unfaded case exists in the more realistic faded channel environment. If it does exist, is this degradation below optimal performance worse, or better than the unfaded AWGN case? How does this impact range? For example, the experimental setup might first involve two radios aligned in direct LOS and separated by a short distance. The BER results collected could then be compared to the expected results of a noncoherent BFSK radio operating in a Ricean fading channel. A similar test could then be conducted for the Rayleigh fading channel by including obstacles in the path separating the two radios. Because of the BER characteristics of a fading channel, this experiment would have to be conducted over a larger range of signal-to-noise power in order to investigate the errors in the range that are acceptable for data communications. These results, added to the laboratory results of this thesis, would provide a comprehensive analysis of the radio's physical layer.

Additionally, an in-depth analysis of the SINCGARS receiver at the sub-component level could be performed in order to reveal the cause of the sub-optimal performance or to develop alternative hardware that would receive the SINCGARS signal in a near-optimum way. Such a receiver would have to be backward compatible with current SINCGARS transmitters and be tested to evaluate its ability to receive a SINCGARS signal in AWGN, Ricean, and Rayleigh channels. Capt Juan Svenningsen, also an NPS student, is currently developing a SINCGARS model using Field Programmable Gate Arrays (FPGA) that could be used as a starting point for future work in exploring the hardware aspects of the radio's performance [19].

LIST OF REFERENCES

[1] Max Green, "Tactical VHF Data Communication Improvement Project", Unpublished report prepared by the Marine Corps Tactical Systems Support Activity, 2004.

[2] Williamson, John (Ed.), *Jane's Military Communications 2004-2005*, Jane's Information Group, Surrey, England, 2004.

[3] Air Land Sea Application Center, *FM 6-02.72 (FM 11-1) Tactical Radios*, Langley AFB Virginia, 2002.

[4] Harris Corporation, Radio Communications in the Digital Age Volume Two, June 2000. http://www.rfcomm.harris.com/products/tactical-radio-communications (last accessed 15 Nov 2004)

[5] Michael McCorquodale, Ark-Chew Wong, Karthik Nagarajan, Haluk Kulah, and ClarkT.-C. Nguyen, "An Integrated MEMS-BiCMOS SINCGARS Transceiver", Design Automation Conference 2000, Los Angeles, June 2000.

[6] Bradley J. Hamilton, "SINCGARS System Improvement Program (SIP): Specific Radio Improvements", *1996 Tactical Communication Conference Proceedings*, pp. 397-406, Aug. 1996.

[7] Bernard Sklar, *Digital Communications*, 2nd Edition, Prentice Hall, Upper Saddle River, New Jersey, 2001.

[8] Frank Kragh, Course Notes for EC3510 (Communications Engineering), Naval Postgraduate School, 2004 (unpublished).

[9] Clark Robertson, Course Notes for EC4550 (Digital Communications), Naval Postgraduate School, 2004 (unpublished).

[10] Anthony D. Whalen, *Detection of Signals in Noise*, Academic Press, San Diego, 1971.

[11] John G. Proakis, *Digital Communications*, 4th Edition, McGraw-Hill, New York, 2001.

[12] Peyton Z. Peebles Jr., *Probability, Random Variables, and Random Signal Principles*, 4th Edition, McGraw-Hill, New York, 2001.

[13] Clark Robertson, Course Notes for EC4560 (Communications Electronic Counter Counter Measures (ECCM)), Naval Postgraduate School, 2004 (unpublished).

[14] *Simulink Users Guide*, The Math Works, Natick, Massachusetts, 2004.

[15] *MATLAB Users Guide*, The Math Works, Natick, Massachusetts, 2004.

[16] Floyd M. Gardner and John D. Baker, *Simulation Techniques*, John Wiley and Sons Inc., New York, 1997.

[17] Theodore S. Rappaport, *Wireless Communications*, 2nd Edition, Prentice Hall, Upper Saddle River, New Jersey, 2002.

[18] BER Test Tool: Programmers Guide, Marine Corps Tactical Systems Support Activity, Camp Pendleton, May 2005.

[19] J.P. Svenningsen, "Modeling, Simulation, and Implementation of a Noncoherent Binary Frequency Shift Keying (BFSK) Receiver-Transmitter Into a Field Programmable Gate Array (FPGA)", Master's thesis, Naval Postgraduate School, Monterey, California, 2005.

INITIAL DISTRIBUTION LIST

1. Defense Technical Information Center
   Ft. Belvoir, Virginia

2. Dudley Knox Library
   Naval Postgraduate School
   Monterey, California

3. Marine Corps Representative
   Naval Postgraduate School
   Monterey, California

4. Director, Training and Education, MCCDC, Code C46
   Quantico, Virginia

5. Director, Marine Corps Research Center, MCCDC, Code C40RC
   Quantico, Virginia

6. Marine Corps Tactical Systems Support Activity (Attn: Operations Officer)
   Camp Pendleton, California

7. Chair, Department of Electrical and Computer Engineering
   Naval Postgraduate School
   Monterey, California

8. Dr. Frank Kragh
   Naval Postgraduate School
   Monterey, California

9. Dr. Herschel Loomis
   Naval Postgraduate School
   Monterey, California

10. Dr. Clark Robertson
    Naval Postgraduate School
    Monterey, California

11. Capt Max Greene, USMC
    Marine Corps Tactical Systems Support Activity
    Camp Pendleton, California